Comput Mech (2009) 43:369–391
DOI 10.1007/s00466-008-0311-1

ORIGINAL PAPER

A novel FEM by scaling the gradient of strains with factor α (αFEM)

G. R. Liu · T. Nguyen-Thoi · K. Y. Lam

Received: 1 November 2007 / Accepted: 29 May 2008 / Published online: 1 July 2008

Abstract This paper presents a novel finite element method of quadrilateral elements by scaling the gradient of strains and Jacobian matrices with a scaling factor α (αFEM). We first prove that the solution of the αFEM is continuous for $\alpha \in [0, 1]$ and bounded from both below and above, and hence is convergent. A general procedure of the αFEM has been proposed to obtain the exact or best possible solution for a given problem, in which an exact-α approach is devised for overestimation problems and a zero-α approach is suggested for underestimation problems. Using the proposed αFEM approaches, much more stable and accurate solutions can be obtained compared to that of standard FEM. The theoretical analyses and intensive numerical studies also demonstrate that the αFEM effectively overcomes the following well-known drawbacks of the standard FEM: (1) Overestimation of stiffness matrix when the full Gauss integration is used; (2) Instability problem known as hour-glass locking (presence of hour-glass modes or spurious zero-energy modes) when the reduced integration is used; (3) Volumetric locking in nearly incompressible problems when the bulk modulus becomes infinite.

G. R. Liu · T. Nguyen-Thoi (✉)
Center for Advanced Computations in Engineering Science (ACES), Department of Mechanical Engineering, National University of Singapore, 9 Engineering Drive 1, Singapore 117576, Singapore
e-mail: g0500347@nus.edu.sg

G. R. Liu
Singapore-MIT Alliance (SMA), E4-04-10, 4 Engineering Drive 3, Singapore 117576, Singapore

K. Y. Lam
School of Mechanical and Aerospace Engineering, Nanyang Technological University, 50 Nanyang Avenue, Singapore 639798, Singapore

Keywords Finite element method (FEM) · Alpha finite element method (αFEM) · Exact-α approach · Zero-α approach · Small-α approach

1 Introduction

The finite element method (FEM) has been developed into a reliable, robust and effective technique for engineering problems [23,43]. It is now widely used in engineering design of structural systems due to its versatility for solids and structures of complex geometry and its applicability for many types of non-linear problems.

In solving practical engineering problems, the lower-order quadrilateral isoparametric elements are most popular and widely used for simplicity, accuracy and efficiency. However, they have the following well known drawbacks: (1) When the full Gauss integration is used, the FEM model is in general "overly-stiff" with the internal strain energy being underestimated. (2) They exhibit instability observed as hour-glass modes or spurious zero-energy modes when the reduced integration is used. (3) They lock in nearly incompressible problems when the bulk modulus becomes infinite. In order to overcome these drawbacks, various techniques have been used for each kind. For the first drawback, many assumed strain or mixed models have been proposed in the past decades to reduce the stiffness of the standard FEM model [2,8,22,24,28,29,31,32,34,35,37,40,42]. In these models, the assumed displacement field is identical to that of the standard FEM model, while the strain (hence the stress) field is assumed independent of the assumed displacement field.

Reduced integration technique has also been used to reduce the stiffness of model [17,19,36,44]. However this technique can lead to instability known as the hour-glass

phenominon. To overcome the instability problem or to suppress the zero-energy hour-glass modes, the addition of a stabilization matrix need to be introduced [4–7,15,21,25–27,33]. This stabilization matrix should preserve the conditions of invariance and consistency which ensure that the element passes the patch test. The stabilization matrix also should not contribute to any deformation modes other than the hourglass modes. The stabilization matrices have been developed from the approaches based on the stabilization parameters to the approaches which do not include artificial stabilization parameters. These latest approaches use Taylor expansion of the non-constant part of the shape function derivatives for variationaly consistent stabilization [21,26].

To overcome the volumetric locking in nearly incompressible problems, the first common technique is to use selective reduced integration [17,30]. The idea of this technique is to decompose the material property matrix into two parts, volume part and remaining part, and the stiffness matrix is also decomposed into two parts correspondingly. The reduced integration is then used only on volume-part and the full Gauss integration is used on the remaining part. The second technique is B-bar method which is generalized from the selective integration procedures to anisotropic and nonlinear media by Hughes [16,17]. The idea of this technique is to improve dilatational part of strain-displacement matrix by using reduced integration and then the full Gauss integration is still used to calculate the stiffness matrix from "improved" strain-displacement matrix.

To find a technique, still in the frame work of FEM using the same form of Galerkin weak form, and to effectively overcome the above drawbacks of FEM, we propose a finite element method of quadrilateral elements by scaling the gradient of strains and Jacobian matrices with a scaling factor α (αFEM). We first show that the αFEM is clearly different from the existing techniques mentioned above, and the formulation is even variationally inconsistent! We then prove that the solution of the αFEM is a continuous function for $\alpha \in [0,\ 1]$, is bounded from both below and above, and hence converges perfectly. This proof is further confirmed by showing that the present αFEM can always pass the standard patch test for any $\alpha \in [0,\ 1]$, and detailed eigenvalue analyses. Next, a general procedure of the αFEM has been proposed to obtain the exact or best possible solution for a given problem, in which an exact-α approach is devised for overestimation problems and a zero-α approach is suggested for underestimation problems. Using the proposed αFEM approaches, we will obtain much more stable and accurate solutions compared to that of standard FEM. The theoretical analyses and intensive numerical studies have demonstrated that the αFEM effectively overcomes all the above mentioned three drawbacks of standard FEM. Finally, based on our intensive theoretical and numerical study in this work, we put forward our argument that "variation consitency is not a necessary condition for a numerical method". A variationally inconsistent method can well converge, have good properties and produce more accurate solutions compared to the variationally consistent counterpart. Furthermore it is also true that "variational consitency is also not a sufficient condition for a stable numerical method". A well-known example is the quadrilateral FEM element with reduced integration, which is unstable for the overestimation problems.

The paper is outlined as follows. In Sect. 2, the idea of the αFEM is introduced. In Sect. 3, variational principle for examining the αFEM is performed. Some theoretical properties of the αFEM are presented and proven in Sect. 4. Numerical implementation issues and examination are discussed in Sect. 5. In Sect. 6, some numerical examples are conducted and discussed to verify the formulations and properties of the αFEM. Some concluding remarks are made in the Sect. 7.

2 The idea of the αFEM

2.1 Briefing on the finite element method (FEM)(see, e.g. [3,17,18,23,43])

The discrete equations of FEM are generated from the Galerkin weak form

$$\int_{\Omega} (\nabla_s \delta \mathbf{u})^T \mathbf{D} (\nabla_s \mathbf{u}) \, d\Omega - \int_{\Omega} \delta \mathbf{u}^T \mathbf{b} d\Omega - \int_{\Gamma_t} \delta \mathbf{u}^T \bar{\mathbf{t}} d\Gamma = 0 \tag{1}$$

where $\mathbf{b}$ is the vector of external body forces, $\mathbf{D}$ is a symmetric positive definite (SPD) matrix of material constants, $\bar{\mathbf{t}} = \left\{\bar{t}_x \ \bar{t}_y\right\}^T$ is the prescribed traction vector on the natural boundary Γ_t, $\mathbf{u}$ is trial functions, $\delta\mathbf{u}$ is test functions and $\nabla_s \mathbf{u}$ is the symmetric gradient of the displacement field.

The FEM uses the following trial and test functions

$$\mathbf{u}^h (\mathbf{x}) = \sum_{I=1}^{\mathrm{NP}} \mathbf{N}_I (\mathbf{x}) \, \mathbf{d}_I; \quad \delta \mathbf{u}^h (\mathbf{x}) = \sum_{I=1}^{\mathrm{NP}} \mathbf{N}_I (\mathbf{x}) \, \delta \mathbf{d}_I \tag{2}$$

where NP is the number of the nodal variables of the element, $\mathbf{d}_I = [u_I \ v_I]^T$ is the nodal displacement vector and $\mathbf{N}_I(\mathbf{x}) = \begin{bmatrix} N_I(\mathbf{x}) & 0 \\ 0 & N_I(\mathbf{x}) \end{bmatrix}$ is the shape function matrix.

By substituting the approximations, $\mathbf{u}^h$ and $\delta\mathbf{u}^h$, into the weak form and invoking the arbitrariness of virtual nodal displacements, Eq. (1) yields the standard discretized algebraic equation system:

$$\mathbf{K}^{\mathrm{FEM}} \mathbf{d} = \mathbf{f} \tag{3}$$

where $\mathbf{K}^{\text{FEM}}$ is the stiffness matrix, $\mathbf{f}$ is the element force vector, that are assembled with entries of

$$\mathbf{K}_{IJ}^{\text{FEM}} = \int_{\Omega} \mathbf{B}_I^T \mathbf{D}\mathbf{B}_J d\Omega \tag{4}$$

$$\mathbf{f}_I = \int_{\Omega} \mathbf{N}_I^T(\mathbf{x})\mathbf{b}d\Omega + \int_{\Gamma_t} \mathbf{N}_I^T(\mathbf{x})\bar{\mathbf{t}}d\Gamma \tag{5}$$

with the *strain matrix* defined as

$$\mathbf{B}_I(\mathbf{x}) = \nabla_s N_I(\mathbf{x}) \tag{6}$$

In numerical performance, the isoparametric elements and Gauss integration are usually used to calculate the entries of stiffness matrix $\mathbf{K}_{IJ}^{\text{FEM}}$ as follows

$$\begin{aligned}\mathbf{K}_{IJ}^{\text{FEM}} &= \int_{\Omega} \mathbf{B}_I^T(\mathbf{x})\,\mathbf{D}\mathbf{B}_J(\mathbf{x})\,d\Omega \\ &= \int_{-1}^{1}\int_{-1}^{1} \mathbf{B}_I^T(\mathbf{x}(\xi,\eta))\,\mathbf{D}\mathbf{B}_J(\mathbf{x}(\xi,\eta))\,|\mathbf{J}(\xi,\eta)|\,d\xi d\eta \\ &= \sum_{i=1}^{M_1}\sum_{j=1}^{M_2} \mathbf{B}_I^T\left(\mathbf{x}\left(\xi_i,\eta_j\right)\right)\mathbf{D}\mathbf{B}_J \\ &\quad \times \left(\mathbf{x}\left(\xi_i,\eta_j\right)\right)\left|\mathbf{J}\left(\xi_i,\eta_j\right)\right| W_i \bar{W}_j\end{aligned} \tag{7}$$

where M_1 and M_2 are the number of Gauss integration points in the ξ and η axes, respectively. In addition, $\left(\xi_i,\eta_j\right)$ are the integration points and W_i and $\bar{W}_j$ are weighting coefficients.

2.2 The alpha finite element method (αFEM)

The αFEM is quite similar to the existing standard FEM procedure, except in calculating numerically the stiffness matrix, we will substitute the strain gradient matrix $\mathbf{B}_I(\mathbf{x})$ and the Jacobi matrix $\mathbf{J}(\xi,\eta)$ of standard FEM by a scaled strain matrix $\tilde{\mathbf{B}}_I(\mathbf{x})$ and a corresponding scaled Jacobi matrix $\tilde{\mathbf{J}}$, respectively.

Consider quadrilateral elements and to write explicitly the scaled strain matrix $\tilde{\mathbf{B}}_I(\mathbf{x})$ and the corresponding scaled Jacobi matrix $\tilde{\mathbf{J}}$, we need to rewrite the strain vector $\boldsymbol{\varepsilon}^h$ and the Jacobi matrix $\mathbf{J}(\xi,\eta)$ of standard FEM in other forms. First, the strain vector $\boldsymbol{\varepsilon}^h$ can be rewritten in the summation form of a constant part $\boldsymbol{\varepsilon}_c^h$ and $\boldsymbol{\varepsilon}_v^h(\xi,\eta)$ containing variables $\xi,\ \eta$ as follows

$$\begin{aligned}\boldsymbol{\varepsilon}^h(\mathbf{x}(\xi,\eta)) &= \nabla_s \mathbf{u}^h = \sum_{I=1}^{\text{NP}} \mathbf{B}_I(\mathbf{x}(\xi,\eta))\,\mathbf{d}_I \\ &= \boldsymbol{\varepsilon}_c^h + \boldsymbol{\varepsilon}_v^h(\xi,\eta)\end{aligned} \tag{8}$$

For the bilinear isoparametric element, $\boldsymbol{\varepsilon}_c^h$ and $\boldsymbol{\varepsilon}_v^h(\xi,\eta)$ have the following forms

$$\boldsymbol{\varepsilon}_c^h = \begin{Bmatrix}\varepsilon_{c1}\\ \varepsilon_{c2}\\ \varepsilon_{c3}\end{Bmatrix} \quad \text{and} \quad \boldsymbol{\varepsilon}_v^h = \begin{Bmatrix}\eta\varepsilon_{v1}\\ \xi\varepsilon_{v2}\\ \xi\varepsilon_{v1}+\eta\varepsilon_{v2}\end{Bmatrix} \tag{9}$$

where $\varepsilon_{c1}, \varepsilon_{c2}, \varepsilon_{c3}, \varepsilon_{v1}$ and ε_{v2} are scalars depending on the displacement of nodes of the element.

Correspondingly, the Jacobian matrix $\mathbf{J}(\xi,\eta)$ is rewritten in the summation form of a constant part $\mathbf{J}_c$ and $\mathbf{J}_v(\xi,\eta)$ containing variables $\xi,\ \eta$ as follows

$$\mathbf{J}(\xi,\eta) = \mathbf{J}_c + \mathbf{J}_v(\xi,\eta) \tag{10}$$

In the αFEM, the following "scaled strain" is used

$$\begin{aligned}\tilde{\boldsymbol{\varepsilon}}^h(\alpha,\xi,\eta) &= \tilde{\mathbf{B}}\mathbf{d} = \sum_{I=1}^{\text{NP}} \tilde{\mathbf{B}}_I(\mathbf{x}(\alpha,\xi,\eta))\mathbf{d}_I \\ &= \boldsymbol{\varepsilon}_c^h + \alpha\boldsymbol{\varepsilon}_v^h(\xi,\eta)\end{aligned} \tag{11}$$

where $\alpha \in [0,1]$ is a scaling factor, and $\boldsymbol{\varepsilon}_c^h, \boldsymbol{\varepsilon}_v^h(\xi,\eta)$ are components of the strain vector $\boldsymbol{\varepsilon}^h$ of the standard FEM in Eq. (8). In Eq. (11), $\tilde{\mathbf{B}}$ is the scaled strain matrix which is written in the summation form of a constant part $\mathbf{B}_c$ and $\mathbf{B}_v(\xi,\eta)$ containing variables $\xi,\ \eta$ as follows

$$\tilde{\mathbf{B}} = \mathbf{B}_c + \alpha\mathbf{B}_v(\xi,\eta) \tag{12}$$

Correspondingly, the scaled Jacobian matrix $\tilde{\mathbf{J}}(\alpha,\xi,\eta)$ is now also "scaled" as follows

$$\tilde{\mathbf{J}}(\alpha,\xi,\eta) = \mathbf{J}_c + \alpha\mathbf{J}_v(\xi,\eta) \tag{13}$$

where $\mathbf{J}_c$ and $\mathbf{J}_v(\xi,\eta)$ are components of the Jacobian matrix $\mathbf{J}(\xi,\eta)$ in Eq. (10). Note again that the scaling is only on the gradient of the Jacobian matrix.

The final discretized algebraic equation system of the αFEM has the form of

$$\mathbf{K}^{\alpha\text{FEM}}\mathbf{d} = \mathbf{f} \tag{14}$$

where $\mathbf{K}^{\alpha\text{FEM}}$ is the stiffness matrix. In numerical performance using the isoparametric elements and Gauss integration, the entries of scaled stiffness matrix $\mathbf{K}_{IJ}^{\alpha\text{FEM}}$ become

$$\begin{aligned}\mathbf{K}_{IJ}^{\alpha\text{FEM}} &= \int_{-1}^{1}\int_{-1}^{1} \tilde{\mathbf{B}}_I^T(\mathbf{x}(\alpha,\xi,\eta))\,\mathbf{D}\tilde{\mathbf{B}}_J \\ &\quad \times (\mathbf{x}(\alpha,\xi,\eta))\left|\tilde{\mathbf{J}}(\alpha,\xi,\eta)\right| d\xi d\eta \\ &= \sum_{i=1}^{M_1}\sum_{j=1}^{M_2} \tilde{\mathbf{B}}_I^T\left(\mathbf{x}\left(\alpha,\xi_i,\eta_j\right)\right)\mathbf{D}\tilde{\mathbf{B}}_J \\ &\quad \times \left(\mathbf{x}\left(\alpha,\xi_i,\eta_j\right)\right)\left|\tilde{\mathbf{J}}\left(\alpha,\xi_i,\eta_j\right)\right| W_i\bar{W}_j\end{aligned} \tag{15}$$

and $\mathbf{f}$ is the element force vector which is the same to that of the standard FEM.

In the αFEM, we will always use full Gauss integration that is 2 by 2 or $G = 4$ for quadrilateral elements, and the solution of the αFEM will change depending on the value of scaling factor $\alpha \in [0,\ 1]$. Note that the scaling to the strains is performed for both the evaluation of stiffness matrix and for computing the strains after the displacement is obtained.

3 Variational principle for examining the αFEM

In the αFEM, the Galerkin weak form is used with the scaled strain (11) instead of the consistent strain (8), the variational consistency needs to be examined. To this end, we start with the modified Hellinger–Reissner variational principle with the assumed strain vector $\tilde{\boldsymbol{\varepsilon}}$ and displacements $\mathbf{u}$ as independent field variables [32]:

$$U(\mathbf{u}, \tilde{\boldsymbol{\varepsilon}}) = -\int_{\Omega} \frac{1}{2}\tilde{\boldsymbol{\varepsilon}}^T \mathbf{D}\tilde{\boldsymbol{\varepsilon}} d\Omega + \int_{\Omega} (\mathbf{D}\tilde{\boldsymbol{\varepsilon}})^T (\nabla_s \mathbf{u}) d\Omega - \int_{\Omega} \mathbf{u}^T \mathbf{b} d\Omega - \int_{\Gamma_t} \mathbf{u}^T \bar{\mathbf{t}} d\Gamma \tag{16}$$

Performing the variation using the chain rule, one obtains

$$\delta U(\mathbf{u}, \tilde{\boldsymbol{\varepsilon}}) = -\int_{\Omega} \delta\tilde{\boldsymbol{\varepsilon}}^T \mathbf{D}\tilde{\boldsymbol{\varepsilon}} d\Omega + \int_{\Omega} \delta\tilde{\boldsymbol{\varepsilon}}^T \mathbf{D}(\nabla_s \mathbf{u}) d\Omega + \int_{\Omega} \tilde{\boldsymbol{\varepsilon}}^T \mathbf{D}(\nabla_s \delta\mathbf{u}) d\Omega - \int_{\Omega} \delta\mathbf{u}^T \mathbf{b} d\Omega - \int_{\Gamma_t} \delta\mathbf{u}^T \bar{\mathbf{t}} d\Gamma = 0 \tag{17}$$

Substituting the approximations (2), (11) into (17) and use the scaled Jacobian matrix $\tilde{\mathbf{J}}(\alpha, \xi, \eta)$ in (13) instead the standard Jacobian matrix $\mathbf{J}(\xi, \eta)$ in calculating the integrals using isoparametric elements, and using the arbitrary property of variation, we obtain

$$\mathbf{K}^{\text{two-field}}\mathbf{d} = \mathbf{f} \tag{18}$$

where $\mathbf{K}^{\text{two-field}}$ is the *assumed* stiffness matrix, and $\mathbf{f}$ is the element force vector given by

$$\mathbf{K}_{IJ}^{\text{two-field}} = -\int_{-1}^{1}\int_{-1}^{1} \tilde{\mathbf{B}}_I^T \mathbf{D}\tilde{\mathbf{B}}_J \left|\tilde{\mathbf{J}}(\alpha, \xi, \eta)\right| d\xi d\eta + 2\int_{-1}^{1}\int_{-1}^{1} \tilde{\mathbf{B}}_I^T \mathbf{D}\mathbf{B}_J \left|\tilde{\mathbf{J}}(\alpha, \xi, \eta)\right| d\xi d\eta \tag{19}$$

$$\mathbf{f}_I = \int_{\Omega} \mathbf{N}_I^T(\mathbf{x})\mathbf{b} d\Omega + \int_{\Gamma_t} \mathbf{N}_I^T(\mathbf{x})\bar{\mathbf{t}} d\Gamma \tag{20}$$

Only when the condition

$$\int_{-1}^{1}\int_{-1}^{1} \tilde{\mathbf{B}}_I^T \mathbf{D}\tilde{\mathbf{B}}_J \left|\tilde{\mathbf{J}}(\alpha, \xi, \eta)\right| d\xi d\eta = \int_{-1}^{1}\int_{-1}^{1} \tilde{\mathbf{B}}_I^T \mathbf{D}\mathbf{B}_J \left|\tilde{\mathbf{J}}(\alpha, \xi, \eta)\right| d\xi d\eta \tag{21}$$

is satisfied, from Eq. (19) we then have

$$\mathbf{K}_{IJ}^{\text{two-field}} = \int_{-1}^{1}\int_{-1}^{1} \tilde{\mathbf{B}}_I^T \mathbf{D}\tilde{\mathbf{B}}_J \left|\tilde{\mathbf{J}}(\alpha, \xi, \eta)\right| d\xi d\eta \tag{22}$$

The αFEM uses directly Eq. (22) to calculate the stiffness matrix regardless whether or not the conditions (21) and $\left|\tilde{\mathbf{J}}(\alpha, \xi, \eta)\right| = |\mathbf{J}(\xi, \eta)|$ are satisfied. Therefore, the αFEM may or may not be "variationally consistent", and hence its properties need to be examined to prove its stability and convergence. Note that Eq. (21) is a special case of the so-call orthogonal condition [37].

The αFEM is some what similar to the SFEM [22,24], in terms of making use of the discovered fact that "the gradient of the *compatible* strain field does not have to be kept exactly and can be properly manipulated". Such a manipulation and the resulted stress field via the constitute equation $\sigma = \mathbf{D}\tilde{\boldsymbol{\varepsilon}}$ usually do not satisfy the orthogonal condition in general, and result in a violation of the variational principle, meaning that the same form of the Galerkin weak form used for such a manipulated strain field may not be derived from the Hu-Washizu or modified Hellinger–Reissner principles. However different from the SFEM, the αFEM gives much better and simple way to manipulate the strain field by simply scaling the *gradient* part of the compatible strain field by a scaling factor α, and this scaled strain field still satisfies two criteria for a Galerkin weak form to converge: (1) a compatible displacement filed (in H^1 space) has to be assumed; (2) the constant part of the strain field of the *compatible* strain field from the assumed displacement field has to be exactly captured.

4 Properties of the αFEM

4.1 Variational consistency and energy consistency

Remark 1 When $\alpha = 1.0$, the αFEM becomes the standard FEM using full Gauss integration ($G = 4$). It is v*ariationally consistent* and $\mathbf{K}_{IJ(\alpha=1)}^{\alpha\text{FEM}} = \mathbf{K}_{IJ(G=4)}^{\text{FEM}}$.

Remark 2 When $\alpha = 0.0$, the αFEM becomes the standard FEM using reduced integration. It is variationally consistent and $\mathbf{K}_{IJ(\alpha=0)}^{\alpha\text{FEM}} = \mathbf{K}_{IJ(G=1)}^{\text{FEM}}$.

Remark 3 When $0.0 < \alpha < 1.0$, we obtain a continuous form of solutions ranging from the standard FEM using reduced integration to that using full Gauss integration. The method is not variationally consistent because Eq. (21) can not be satisfied.

Remark 3 naturally gives rise to a question: is the αFEM solution reliable when $0.0 < \alpha < 1.0$ is used? The following theorem will provide a positive answer.

Theorem 1 *The strain energy function $E(\alpha)$ of the αFEM is a fourth order function of scaling factor α and always gains a local extreme value at $\alpha = 0.0$. This strain energy function satisfies the following bound*

$$E(\alpha = 1.0) < E(\alpha) < E(\alpha = 0.0), \quad \alpha \in (0,\ 1) \tag{23}$$

which implies that the αFEM is energy consistent.

Proof The strain energy function $E(\alpha)$ of the element will be calculated as follows

$$\begin{aligned} E(\alpha) &= \int_{-1}^{1}\int_{-1}^{1}\left(\tilde{\boldsymbol{\varepsilon}}^h(\alpha,\xi,\eta)\right)^T \mathbf{D}\tilde{\boldsymbol{\varepsilon}}^h(\alpha,\xi,\eta)\left|\tilde{\mathbf{J}}(\alpha,\xi,\eta)\right| d\xi d\eta \\ &= \int_{-1}^{1}\int_{-1}^{1}\left(\alpha\boldsymbol{\varepsilon}_v^h(\xi,\eta)+\boldsymbol{\varepsilon}_c^h\right)^T \mathbf{D} \\ &\quad \times\left(\alpha\boldsymbol{\varepsilon}_v^h(\xi,\eta)+\boldsymbol{\varepsilon}_c^h\right)\left|\tilde{\mathbf{J}}(\alpha,\xi,\eta)\right| d\xi d\eta \\ &= \alpha^2 E_{vv} + 2\alpha E_{vc} + E_{cc} \end{aligned} \tag{24}$$

where

$$E_{vv} = \int_{-1}^{1}\int_{-1}^{1}\left(\boldsymbol{\varepsilon}_v^h(\xi,\eta)\right)^T \mathbf{D}\boldsymbol{\varepsilon}_v^h(\xi,\eta)\left|\tilde{\mathbf{J}}(\alpha,\xi,\eta)\right| d\xi d\eta \tag{25}$$

$$E_{vc} = \int_{-1}^{1}\int_{-1}^{1}\left(\boldsymbol{\varepsilon}_v^h(\xi,\eta)\right)^T \mathbf{D}\boldsymbol{\varepsilon}_c^h\left|\tilde{\mathbf{J}}(\alpha,\xi,\eta)\right| d\xi d\eta \tag{26}$$

$$E_{cc} = \int_{-1}^{1}\int_{-1}^{1}\left(\boldsymbol{\varepsilon}_c^h\right)^T \mathbf{D}\boldsymbol{\varepsilon}_c^h\left|\tilde{\mathbf{J}}(\alpha,\xi,\eta)\right| d\xi d\eta \tag{27}$$

We now examine E_{vc} in detail. First, the determinant of the Jacobian matrix $\tilde{\mathbf{J}}(\alpha,\xi,\eta)$ is written as follows

$$\left|\tilde{\mathbf{J}}(\alpha,\xi,\eta)\right| = J_1 + J_2\alpha\eta + J_3\alpha\xi + J_4\alpha^2\xi\eta \tag{28}$$

where J_1, J_2, J_3, and J_4 are scalars depending on the coordinate of nodes of the element.

Substituting Eqs. (9), (28) into (26) and use the general form of the material matrix $\boldsymbol{D}$ for the plain strain and plain stress problems, we obtain

$$\begin{aligned} E_{vc} &= \int_{-1}^{1}\int_{-1}^{1}\left(\boldsymbol{\varepsilon}_v^h(\xi,\eta)\right)^T \mathbf{D}\boldsymbol{\varepsilon}_c^h\left|\tilde{\mathbf{J}}(\alpha,\xi,\eta)\right| d\xi d\eta \\ &= \int_{-1}^{1}\int_{-1}^{1}\left\{\eta\varepsilon_{v1} \quad \xi\varepsilon_{v2} \quad \xi\varepsilon_{v1}+\eta\varepsilon_{v2}\right\}\begin{bmatrix} D_{11} & D_{12} & 0 \\ D_{21} & D_{22} & 0 \\ 0 & 0 & D_{33}\end{bmatrix} \\ &\quad \times\begin{Bmatrix}\varepsilon_{c1}\\ \varepsilon_{c2}\\ \varepsilon_{c3}\end{Bmatrix}\left(J_1 + J_2\alpha\eta + J_3\alpha\xi + J_4\alpha^2\xi\eta\right) d\xi d\eta \\ &= \int_{-1}^{1}\int_{-1}^{1}\left(\eta\left(\varepsilon_{v1}\varepsilon_{c1}D_{11} + \varepsilon_{v1}\varepsilon_{c2}D_{21} + \varepsilon_{v2}\varepsilon_{c3}D_{33}\right)\right. \\ &\quad \left. + \xi\left(\varepsilon_{v2}\varepsilon_{c1}D_{21} + \varepsilon_{v2}\varepsilon_{c2}D_{22} + \varepsilon_{v1}\varepsilon_{c3}D_{33}\right)\right) \\ &\quad \times\left(J_1 + J_2\alpha\eta + J_3\alpha\xi + J_4\alpha^2\xi\eta\right) d\xi d\eta \\ &= \int_{-1}^{1}\int_{-1}^{1}(\eta C_1 + \xi C_2)(J_1 + J_2\alpha\eta \\ &\quad + J_3\alpha\xi + J_4\alpha^2\xi\eta) d\xi d\eta \\ &= \int_{-1}^{1}\int_{-1}^{1}\left(C_1J_2\alpha\eta^2 + C_2J_3\alpha\xi^2\right) d\xi d\eta \\ &= \alpha\frac{4}{3}(C_1J_2 + C_2J_3) \end{aligned} \tag{29}$$

where

$$\begin{aligned} C_1 &= \varepsilon_{v1}\varepsilon_{c1}D_{11} + \varepsilon_{v1}\varepsilon_{c2}D_{21} + \varepsilon_{v2}\varepsilon_{c3}D_{33} \\ C_2 &= \varepsilon_{v2}\varepsilon_{c1}D_{21} + \varepsilon_{v2}\varepsilon_{c2}D_{22} + \varepsilon_{v1}\varepsilon_{c3}D_{33} \end{aligned} \tag{30}$$

Note that we used the following results to obtain Eq. (29)

$$\begin{aligned} \int_{-1}^{1}\int_{-1}^{1}\xi d\xi d\eta &= \int_{-1}^{1}\int_{-1}^{1}\eta d\xi d\eta = \int_{-1}^{1}\int_{-1}^{1}\xi\eta d\xi d\eta \\ &= \int_{-1}^{1}\int_{-1}^{1}\xi\eta^2 d\xi d\eta = \int_{-1}^{1}\int_{-1}^{1}\xi^2\eta d\xi d\eta = 0 \end{aligned} \tag{31}$$

Following the same but lengthy procedure, we obtain

$$E_{vv} = \frac{4}{3}(C_3J_1 + C_5J_1) + \frac{4}{9}J_4C_4\alpha^2 \tag{32}$$

$$E_{cc} = C_6J_1 \tag{33}$$

where

$$\begin{aligned} C_3 &= \varepsilon_{v1}^2D_{11} + \varepsilon_{v2}^2D_{33} \\ C_4 &= 2\varepsilon_{v1}\varepsilon_{v2}(D_{21} + D_{33}) \\ C_5 &= \varepsilon_{v2}^2D_{22} + \varepsilon_{v1}^2D_{33} \\ C_6 &= 4\left(\varepsilon_{c1}^2D_{11} + 2\varepsilon_{c1}\varepsilon_{c2}D_{21} + \varepsilon_{c2}^2D_{22} + \varepsilon_{c3}^2D_{33}\right) \end{aligned} \tag{34}$$

Substituting Eqs. (29), (32) and (33) into (24), we obtain

$$\begin{aligned} E(\alpha) &= \alpha^2 \left(\frac{4}{3}(C_3 J_1 + C_5 J_1) + \frac{4}{9} J_4 C_4 \alpha^2 \right) \\ &\quad + 2\alpha\alpha \frac{4}{3}(C_1 J_2 + C_2 J_3) + C_6 J_1 \\ &= \alpha^4 \frac{4}{9} J_4 C_4 + \alpha^2 \left(\frac{4}{3}(C_3 J_1 + C_5 J_1) \right. \\ &\quad \left. + \frac{8}{3}(C_1 J_2 + C_2 J_3) \right) + C_6 J_1 \end{aligned}$$

which has the simple form of

$$E(\alpha) = \alpha^4 F_1 + \alpha^2 F_2 + F_3 \tag{35}$$

where

$$\begin{aligned} F_1 &= \frac{4}{9} J_4 C_4; \\ F_2 &= \frac{4}{3}(C_3 J_1 + C_5 J_1) + \frac{8}{3}(C_1 J_2 + C_2 J_3); \\ F_3 &= C_6 J_1 \end{aligned} \tag{36}$$

Equation (35) shows that the strain energy function $E(\alpha)$ is a fourth order function of scaling factor α. Take derivative of Eq. (35) with respect to scaling factor α, we have

$$\frac{\partial E(\alpha)}{\partial \alpha} = 4\alpha^3 F_1 + 2\alpha F_2 \tag{37}$$

which shows that the strain energy function $E(\alpha)$ always gains a local extreme value at $\alpha = 0.0$.

So far, the results of the standard displacement FEM shows that the strain energy using the reduced integration is always larger than that using the full Gauss integration [17,19] which implies that

$$F_1 + F_2 + F_3 = E(\alpha = 1) < E(\alpha = 0) = F_3 \tag{38}$$

Combining Eq. (38) with the Eq. (35), it is easy to see that

$$E(\alpha = 1) < E(\alpha) < E(\alpha = 0), \quad \alpha \in (0, 1)$$

which implies that the αFEM is *energy consistent*. □

Note that the concept *energy consistent* which was first introduced by Liu et al. [24] implies herein that the strain energy of the αFEM with $\alpha \in (0, 1)$ is finite and bounded from above and below by the strain energies $E(\alpha = 0.0)$ and $E(\alpha = 1.0)$, respectively.

Theorem 1 states that even when the αFEM with $\alpha \in (0, 1)$ is not "variationally consistent" by the definition of Eq. (21), it produces meaningful results that are energy consistent and has bound property given in Eq. (23). Theorem 1 also shows that with $\alpha \in [0, 1]$, the strain energy of the αFEM is biggest at $\alpha = 0.0$, but smallest at $\alpha = 1.0$, and we can reduce the overestimation of stiffness matrix of the standard FEM using the full Gauss integration by using $0.0 \leq \alpha < 1.0$ in the αFEM.

The consistency in energy will ensure the αFEM passes the standard patch test (see, Sect. 5.2) for all $\alpha \in [0, 1]$, which will further confirm that there is no energy loss for any linear fields and the αFEM has linear field re-producibility and hence sufficient to converge to any continuous fields.

4.2 Classification of problems

Depending on boundary conditions, the numerical results of the αFEM with $\alpha = 0.0$ (or the standard FEM using *reduced* integration) have different properties. Based on these properties, we can classify the problems in two groups:

- Overestimation problems: the solution of strain energy obtained using the αFEM with $\alpha = 0.0$ is an "overestimation" of the exact solution.
- Underestimation problems: the solution of strain energy obtained using the αFEM with $\alpha = 0.0$ is an "underestimation" of the exact solution.

Generally, underestimation problems are often significantly over-determined with excessive displacement constraints. The numerical stability is therefore ensured at $\alpha = 0.0$. On the other hand, overestimation problems are under-determined with less displacement constraints. The numerical instability will therefore happen at $\alpha = 0.0$. Note that the classification of problems into over- or underestimation is based on the global energy, not any local quantity. Hence, this classification of problems can be done for any structure.

4.3 Determination of overestimation or underestimation of the exact solution

Note that to determine the αFEM solution at a specific value of α being an underestimation or overestimation of the exact solution is straightforward. All we need is to compute the strain energy $E(\alpha)$ for two coarse meshes of different densities. If $E(\alpha)$ of the finer mesh is larger than that of the coarser mesh, the αFEM solution (in strain energy) is an underestimation of the exact solution. Vice versa, if $E(\alpha)$ of the finer mesh is smaller than that of the coarser mesh, the αFEM solution (in strain energy) is an overestimation of the exact solution.

Note also the fact that, the solution of the αFEM with $\alpha = 1.0$ (or FEM using full Gauss integration) is always an underestimation of that using the αFEM with $\alpha = 0.0$ and the exact solution [17,19]. Combining these results with Remarks 1–3 and Theorem 1, we have two following important theorems on the producibility of the exact solution by the αFEM.

4.4 Producibility of the exact solution by the αFEM

Theorem 2 *If the strain energy of the αFEM solution at $\alpha = 0.0$ is an overestimation of the exact solution, there exists a value of α_{exact} such that*

$$E(\alpha_{\text{exact}}) = E_{\text{exact}} \tag{39}$$

which shows that the strain energy of the αFEM at $\alpha = \alpha_{\text{exact}}$ is equal to the strain energy of the exact solution.

Proof From the Remark 3 and Theorem 1, we see that the energy diagram of the αFEM is a continuous function from $\alpha = 0.0$ to $\alpha = 1.0$. Because the strain energy of the αFEM at $\alpha = 0.0$ is an overestimation of the exact solution, while the strain energy of the αFEM at $\alpha = 1.0$ is an underestimation of the exact solution, therefore there exists a value of α_{exact} such that

$$E(\alpha_{\text{exact}}) = E_{\text{exact}}$$

which shows that the strain energy of the αFEM at $\alpha = \alpha_{\text{exact}}$ is equal to the strain energy of the exact solution. □

4.5 Exact-α approach

Theorem 2 provides the foundation for us to devise an exact-α approach that can be used to find the exact solution using the αFEM for overestimation problems. The exact-α approach works as follows.

a. Use two coarse meshes of same aspect ratio to compute two E(α)-α curves.
b. Obtain the intersection point of these two curves to determine α_{exact} and $E(\alpha_{\text{exact}})$ that is the exact solution of strain energy of the problem (see Sect. 4.6).
c. Create a fine mesh of the same aspect ratio, and using the αFEM with α_{exact} to compute the displacement solution.
d. Use the displacement solution to compute the strains and stresses.

Examples of application of the exact-α approach are presented in Sect. 6.

4.6 Procedure to determine α_{exact}

The above results show that we can use only two coarse meshes of the same aspect ratio to find the solution of which the strain energy is the exact solution. The general procedure to determine α_{exact} is now presented as follows. For one mesh, the strain energy curve $E(\alpha)$ can be determined using three values of $\alpha \in [0,\ 1]$, and using Eq. (35) we have

$$E(\alpha_1) = \alpha_1^4 F_1^{(1)} + \alpha_1^2 F_2^{(1)} + F_3^{(1)}$$
$$E(\alpha_2) = \alpha_2^4 F_1^{(1)} + \alpha_2^2 F_2^{(1)} + F_3^{(1)}$$
$$E(\alpha_3) = \alpha_3^4 F_1^{(1)} + \alpha_3^2 F_2^{(1)} + F_3^{(1)}$$

The above equation set can be solved for $F_1^{(1)}$, $F_2^{(1)}$ and $F_3^{(1)}$, and we then have

$$E(\alpha) = \alpha^4 F_1^{(1)} + \alpha^2 F_2^{(1)} + F_3^{(1)} \tag{40}$$

For another mesh of the same aspect ratio, we can also obtain

$$E(\alpha) = \alpha^4 F_1^{(2)} + \alpha^2 F_2^{(2)} + F_3^{(2)} \tag{41}$$

Finally, $\alpha_{\text{exact}} \in (0,\ 1)$ is obtained by finding the roots for the following equation

$$\alpha^4 \left(F_1^{(1)} - F_1^{(2)}\right) + \alpha^2 \left(F_2^{(1)} - F_2^{(2)}\right) + F_3^{(1)} - F_3^{(2)} = 0 \tag{42}$$

4.7 Zero-α approach

For underestimation problems, we propose a "zero-α approach" that offeres the best possible solution for such problems in energy norm.

Theorem 3 *If the strain energy of the αFEM solution at $\alpha = 0.0$ is an "underestimation" of the exact solution, the strain energy of the αFEM at $\alpha = 0.0$ is closest to the exact strain energy.*

Proof Similar to Theorem 2, from the Remark 3 and Theorem 1, we see that the energy diagram of the αFEM is a continuous function from $\alpha = 0.0$ to $\alpha = 1.0$ and the strain energy satisfies

$$E(\alpha = 1.0) < E(\alpha) < E(\alpha = 0.0), \quad \alpha \in (0,\ 1)$$

which shows that the strain energy $E(\alpha)$ of the αFEM with $\alpha \in (0,\ 1)$ is bounded from above by $E(\alpha = 0.0)$. Because both the strain energies of the αFEM at $\alpha = 0.0$ and $\alpha = 1.0$ are underestimations of the exact solution, the strain energy of the αFEM at $\alpha = 0.0$ is therefore closest to the exact strain energy. □

Theorem 3 provides the foundation for us to use $\alpha = 0.0$ to find the possible best solution in the strain energy for underestimation problems for any discretizations of problem domain. Remind that for the underestimation problems, the numerical stability of the solution at $\alpha = 0.0$ is ensured due to excessive displacement constraints.

4.8 General procedure of the αFEM for a practical problem

Theorems 1–3 ensures that the αFEM can provide a bounded solution (in energy) that is closest to the exact solution. It is also *always* better than the standard FEM solution. We now present a general approach of using the αFEM to solve a practical engineering problem:

a. Use two coarse meshes and $\alpha = 0.0$ to determine the type of the problem: over- or underestimation problem (see, Sect. 4.3);
b. For overestimation problems, use the exact-α approach; for underestimation problems, use the zero-α approach.

Note that, the strain energy is a positive scalar and its relation with respect to α can be found easily. The displacement is a vector of real numbers, and it relates to α through the linear algebra equation system $\mathbf{K}(\alpha)\mathbf{d} = \mathbf{f}$ which can not be expressed explicitly. However, it is always ensured that nothing will go wrong for the displacements for any $\alpha \in (0,\ 1)$ because of the well-conditioned $\mathbf{K}(\alpha)$, and the bounded $\frac{1}{2}\mathbf{d}^T\mathbf{K}(\alpha)\mathbf{d}$.

Note also the solution which is "best" in energy does not guarantee best in displacement. This is common to any numerical methods based on energy principles. The present αFEM is not meant to changes this fact. Our numerical example shows that when the system energy is at the best status, the displacements are generally of good (not the best) accuracy, and always converge (may not be monotonically).

5 Numerical implementation and examination

5.1 Procedure of the αFEM

The numerical procedure for the αFEM is almost similar to that for the standard displacement compatible FEM. We only change a little to calculate the scaled gradient matrix and the scaled Jacobian matrix by adding a scaling factor α to the components of standard strain gradient and Jacobian matrices containing coordinates ξ, η in the isoparametric elements. In the αFEM, we always use full Gauss integration. The change of the scaling factor α from 0.0 to 1.0 gives the different solutions that will be examined in details.

5.2 Standard patch test: linear reproducibility/convergence

Two types of discretization are used, as shown in Fig. 3: one with 10×10 regular elements and the other with irregular interior nodes whose coordinates are generated in the following fashion

$$x' = x + \Delta x \cdot r_c \cdot \alpha_{ir}$$
$$y' = y + \Delta y \cdot r_c \cdot \alpha_{ir} \tag{43}$$

where Δx and Δy are initial regular element sizes in $x-$ and $y-$ directions, respectively. r_c is a computer-generated random number between -1.0 and 1.0 and α_{ir} is a prescribed irregularity factor whose value is chosen between 0.0 and 0.3.

The following error norm in displacements is used to examine the computed results.

$$e_d = \frac{\sum_{i=1}^{\text{ndof}} |u_i - u_i^h|}{\sum_{i=1}^{\text{ndof}} |u_i|} \times 100\% \tag{44}$$

where u_i is the exact solution and u_i^h is the numerical solution.

It is found that the αFEM can pass the standard patch test within machine precision regardless of the value of $\alpha \in [0, 1]$ and α_{ir} used as shown in Table 1. There is no accuracy loss due to the choice of α value.

5.3 Stability analysis

In this sub-section, an intensive eigenvalue analysis is conducted to investigate numerically the properties of the proposed αFEM. The value of α will vary from 0.0 to 1.0. In particular, we also consider the results at a very small α, for example $\alpha = 0.001$, to compare these results with those at $\alpha = 0.0$. First, a free vibration analysis using the single value decomposition technique of a free single distorted quadrilateral element with total of 8 degrees of freedom (DOFs) as shown in Fig. 1 is conducted. Tables 2 and 3 show the eigenvalues and the condition number of stiffness matrix $\mathbf{K}$. The results in Table 2 show that

- There are at least 3 zero eigenvalues correspondingly to three rigid movements of the element.
- When $\alpha = 0.0$, two additional zero-energy modes are observed as expected. These two modes correspond to the well known two "hour-glass" modes which are the root of instability in the numerical results.
- As long as $0.0 < \alpha \leq 1.0$, there will be no "spurious" modes, which confirms that the αFEM will be stable when $0.0 < \alpha \leq 1.0$.

Table 1 Displacement error norm $e_d(\%)$

	$\alpha = 0.0$ (FEM(G=1))	$\alpha = 0.2$	$\alpha = 0.4$	$\alpha = 0.6$	$\alpha = 0.8$	$\alpha = 1.0$ (FEM(G=4))
$\alpha_{ir} = 0.0$ (regular mesh)	2.89 e−12	2.55 e−12	2.85 e−12	2.07 e−12	2.42 e−12	2.18 e−12
$\alpha_{ir} = 0.1$	2.80 e−12	2.29 e−12	2.42 e−12	2.50 e−12	1.89 e−12	1.62 e−12
$\alpha_{ir} = 0.2$	2.66 e−12	2.32 e−12	1.69 e−12	2.51 e−12	2.02 e−12	2.18 e−12
$\alpha_{ir} = 0.3$	2.68 e−12	2.68 e−12	2.84 e−12	1.94 e−12	1.68 e−12	1.93 e−12

Table 2 Eigenvalues of a free solid using one element ($E = 3.0 \times 10^7$, $\nu = 0.3$)

Eigen values	$\alpha = 0.0$ (FEM(G = 1))	$\alpha = 0.001$	$\alpha = 0.2$	$\alpha = 0.4$	$\alpha = 0.6$	$\alpha = 0.8$	$\alpha = 1.0$ (FEM(G = 4))
1	0	0	0	0	0	0	0
2	0	0	0	0	0	0	0
3	0	0	0	0	0	0	0
4	0	0.167 e+2	0.067 e+7	0.266 e+7	0.593 e+7	1.025 e+7	1.471 e+7
5	0	0.196 e+2	0.078 e+7	0.311 e+7	0.691 e+7	1.182 e+7	1.659 e+7
6	2.286 e+7	2.286 e+7	2.292 e+7	2.313 e+7	2.361 e+7	2.473 e+7	2.753 e+7
7	2.317 e+7	2.317 e+7	2.323 e+7	2.343 e+7	2.388 e+7	2.492 e+7	2.782 e+7
8	5.825 e+7	5.825 e+7	5.830 e+7	5.846 e+7	5.878 e+7	5.933 e+7	6.035 e+7

Table 3 Condition number of stiffness matrix **K** of a free solid using one element ($E = 3.0 \times 10^7$, $\nu = 0.3$)

	$\alpha = 0.0$ (FEM(G = 1))	$\alpha = 0.001$	$\alpha = 0.2$	$\alpha = 0.4$	$\alpha = 0.6$	$\alpha = 0.8$	$\alpha = 1.0$ (FEM(G = 4))
Condition number	5.17 e+33	4.05 e+17	1.62 e+17	3.45 e+16	5.38 e+16	5.83 e+17	4.11 e+17

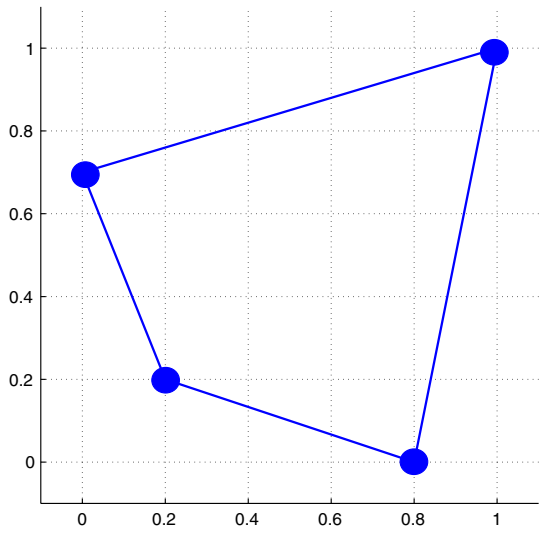

Fig. 1 A distorted quadrilateral element

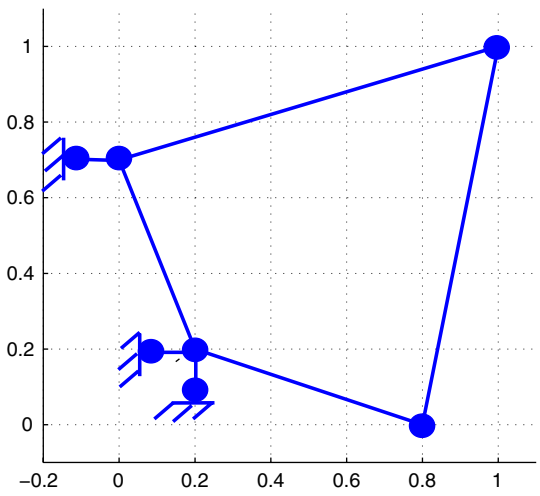

Fig. 2 A single distorted element with 3 fixed DOFs

As shown in Table 3, the condition number of the stiffness matrix **K** is very big at $\alpha = 0.0$, and drastically decreases to much smaller number that are comparable to that at $\alpha = 1.0$ by using any $\alpha > 0$.

Next, we perform a similar vibration analysis for a solid using one distorted element with 3 fixed DOFs as shown in Fig. 2. The results of eigenvalues and condition numbers of matrix **K** are presented in Tables 4 and 5, respectively. The results again show that using any $\alpha > 0$, we can eliminate the spurious zero-energy modes that are observed at $\alpha = 0.0$ (shown in Table 4) and reduce sharply the condition number of matrix **K** which is very big at $\alpha = 0.0$ to much smaller numbers which are comparable with that at $\alpha = 1.0$ (shown in Table 5). In addition, as shown in Table 4, using $\alpha = 0.001$ we will get

- Three 6th, 7th, 8th non-zero eigenvalues that are same to those of the case $\alpha = 0.0$ and
- Two additional 4th, 5th non-zero eigenvalues which replace two spurious zero eigenvalues of $\alpha = 0.0$. These two additional non-zero eigenvalues are larger than 1.0 and very small compared to three above 6th, 7th, 8th non-zero eigenvalues.

The above results imply two important findings for the overestimation problems: (1) there existes a small α_1^{sta}, when $\alpha_1^{\text{sta}} \leq \alpha \leq 1$ the numerical stability (no hour-glass locking) of the present αFEM is always ensured; (2) there existes a small α_2^{sta}, when $\alpha_1^{\text{sta}} \leq \alpha \leq \alpha_2^{\text{sta}}$ the solutions in the strain energy obtained by the present αFEM are almost the same as those of the FEM using the reduced integration.

Table 4 Eigenvalues of a solid with 3 DOFs fixed using one element ($E = 3.0 \times 10^7$, $\nu = 0.3$)

Eigen values	$\alpha = 0.0$ (FEM(G = 1))	$\alpha = 0.001$	$\alpha = 0.2$	$\alpha = 0.4$	$\alpha = 0.6$	$\alpha = 0.8$	$\alpha = 1.0$ (FEM(G = 4))
1	0.0	1.0	1.0	1.0	1.0	1.0	1.0
2	0.0	1.0	1.0	1.0	1.0	1.0	1.0
3	1.0	1.0	1.0	1.0	1.0	1.0	1.0
4	1.0	1.895	0.008 e+7	0.030 e+7	0.065 e+7	0.110 e+7	0.161 e+7
5	1.0	9.508	0.038 e+7	0.153 e+7	0.345 e+7	0.613 e+7	0.943 e+7
6	1.159 e+7	1.159 e+7	1.168 e+7	1.198 e+7	1.252 e+7	1.332 e+7	1.404 e+7
7	1.445 e+7	1.445 e+7	1.446 e+7	1.448 e+7	1.453 e+7	1.469 e+7	1.561 e+7
8	3.995 e+7	3.995 e+7	3.996 e+7	4.001 e+7	4.010 e+7	4.024 e+7	4.043 e+7

Table 5 Condition number of stiffness matrix **K** of a solid with 3 DOFs fixed using one element ($E = 3.0 \times 10^7$, $\nu = 0.3$)

	$\alpha = 0.0$ (FEM(G = 1))	$\alpha = 0.001$	$\alpha = 0.2$	$\alpha = 0.4$	$\alpha = 0.6$	$\alpha = 0.8$	$\alpha = 1.0$ (FEM(G = 4))
Condition number	1.45 e+24	1.82 e+8	1.80 e+8	1.80 e+8	1.80 e+8	1.81 e+8	1.81 e+8

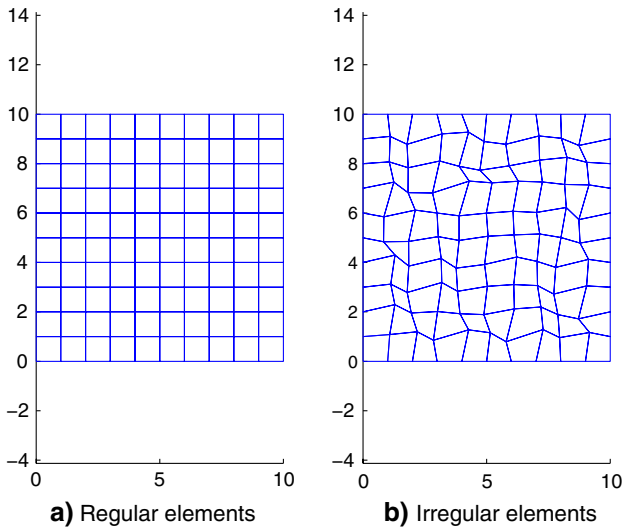

Fig. 3 Domain discretization of a square patch using 4-node quadrilateral elements **a** Regular square elements; **b** Irregular square elements ($\alpha_{ir} = 0.3$)

The question is now how small the α_1^{sta} and α_2^{sta} should be. In order to answer this question in a general manner, we conduct a more detailed study on the two above-mentioned eigenvalue problems, using only very small values of α varying from $\alpha = 1.0e-05$ to $\alpha = 1.0e-01$. The most suitable values of α_1^{sta} and α_2^{sta} should ensure the eigenvalues analysises to satisfy three following conditions: first, the condition number of matrix **K** is comparable to that at $\alpha = 1.0$; second, two additional non-zero eigenvalues which replace spurious zero eigenvalues at $\alpha = 0.0$ should be larger than 1 and as small as possible compared to the others non-zero eigenvalues; third, three non-zero 6th, 7th, 8th eigenvalues should be identical to those at $\alpha = 0.0$. These three conditions will ensure that the stiffness matrix has a good condition number (hence numerical stability) and the results at $\alpha_1^{\text{sta}} \leq \alpha \leq \alpha_2^{\text{sta}}$ in the strain energy are almost the same with those of the FEM using the reduced integration. Tables 6, 7, 8 and 9 show the eigenvalues and the condition number of stiffness matrix **K** versus the various values of α. The results show that $\alpha_1^{\text{sta}} = 1.0e-03$ and $\alpha_2^{\text{sta}} = 1.0e-02$ are the most suitable values of α which satisfy these three conditions.

5.4 αFEM for incompressible materials: small-α approach

Volumetric locking tends to appear when the Poisson's ratio approaches to $^1/_2$. The application of the reduced integration of the standard FEM can avoid such locking. However using the reduced integration in the overestimation problems results in the zero-energy modes or numerical instability, which limits its applications in practice. Using the αFEM with $\alpha_1^{\text{sta}} \leq \alpha \leq \alpha_2^{\text{sta}}$ as presented in Sect. 5.3, we can eliminate this numerical instability. However, the results obtained for α_1^{sta} and α_2^{sta} are for compressible material. It is therefore necessary to conduct again the eigenvalue analysis to find the new stable range $\left[\alpha_1^{\text{vol}},\ \alpha_2^{\text{vol}}\right]$ for the nearly incompressible materials with Poisson's ratio changed from $\nu = 0.499$ to $\nu = 0.499999$. For the new eigenvalue analysis, the small values of α are changed from $\alpha = (0.5 - \nu)\, e - 02$ to $\alpha = (0.5 - \nu)\, e + 02$, where ν is the Poisson ratio. The most suitable values of α_1^{vol} and α_2^{vol} should also ensure the eigenvalues analysises satisfying the three conditions presented in Sect. 5.3.

Tables 10, 11, 12, 13 and 14 show the eigenvalues and the condition number of stiffness matrix **K** versus the various

Table 6 Eigenvalues of a free solid using one element ($E = 3.0 \times 10^7$, $\nu = 0.3$)

Eigen values	$\alpha = 0.0$ (FEM(G = 1))	$\alpha = 1e-05$	$\alpha = 1e-04$	$\alpha = 1e-03$	$\alpha = 1e-02$	$\alpha = 1e-01$	$\alpha = 1.0$ (FEM(G = 4))
1	0.0	0.0	0.0	0.0	0.0	0.0	0.0
2	0.0	0.0	0.0	0.0	0.0	0.0	0.0
3	0.0	0.0	0.0	0.0	0.0	0.0	0.0
4	0.0	0.167 e−02	0.167	0.167 e+2	0.167 e+4	0.167 e+6	1.471 e+7
5	0.0	0.196 e−02	0.196	0.196 e+2	0.196 e+4	0.196 e+6	1.659 e+7
6	2.286 e+7	2.286 e+7	2.286 e+7	2.286 e+7	2.286 e+7	2.287 e+7	2.753 e+7
7	2.317 e+7	2.317 e+7	2.317 e+7	2.317 e+7	2.317 e+7	2.319 e+7	2.782 e+7
8	5.825 e+7	5.825 e+7	5.825 e+7	5.825 e+7	5.825 e+7	5.826 e+7	6.035 e+7

Table 7 Condition number of stiffness matrix **K**of a free solid using one element ($E = 3.0 \times 10^7$, $\nu = 0.3$)

	$\alpha = 0.0$ (FEM(G = 1))	$\alpha = 1e-05$	$\alpha = 1e-04$	$\alpha = 1e-03$	$\alpha = 1e-02$	$\alpha = 1e-01$	$\alpha = 1.0$ (FEM(G = 4))
Condition number	5.174 e+33	5.07 e+17	1.12 e+17	4.05 e+17	0.92 e+17	2.71 e+17	4.11 e+17

Table 8 Eigenvalues of a solid using one element with 3 DOFs fixed ($E = 3.0 \times 10^7$, $\nu = 0.3$)

Eigen values	$\alpha = 0.0$ (FEM(G = 1))	$\alpha = 1e-05$	$\alpha = 1e-04$	$\alpha = 1e-03$	$\alpha = 1e-02$	$\alpha = 1e-01$	$\alpha = 1.0$ (FEM(G = 4))
1	0.0	1.0	1.0	1.0	1.0	1.0	1.0
2	0.0	1.0	1.0	1.0	1.0	1.0	1.0
3	1.0	1.0	1.0	1.0	1.0	1.0	1.0
4	1.0	0.190 e−03	0.190 e−1	0.190 e+1	0.190 e+3	0.189 e+5	0.161 e+7
5	1.0	0.951 e−03	0.951 e−1	0.951 e+1	0.951 e+3	0.951 e+5	0.943 e+7
6	1.159 e+7	1.159 e+7	1.159 e+7	1.159 e+7	1.159 e+7	1.161 e+7	1.404 e+7
7	1.445 e+7	1.445 e+7	1.445 e+7	1.445 e+7	1.445 e+7	1.445 e+7	1.561 e+7
8	3.995 e+7	3.995 e+7	3.995 e+7	3.995 e+7	3.995 e+7	3.995 e+7	4.043 e+7

Table 9 Condition number of stiffness matrix **K** of a solid using one element with 3 DOFs fixed ($E = 3.0 \times 10^7$, $\nu = 0.3$)

	$\alpha = 0.0$ (FEM(G = 1))	$\alpha = 1e-05$	$\alpha = 1e-04$	$\alpha = 1e-03$	$\alpha = 1e-02$	$\alpha = 1e-01$	$\alpha = 1.0$ (FEM(G = 4))
Condition number	1.45 e+24	2.50 e+11	2.51 e+9	1.82 e+8	1.80 e+8	1.80 e+8	1.81 e+8

values of α of the free solid using one element as shown in Fig. 1. The results show that $\alpha_1^{\text{vol}} = (0.5 - \nu)$ and $\alpha_2^{\text{vol}} = (0.5 - \nu)\, e + 01$ are the most suitable values of α for the nearly incompressible materials.

The results of α_1^{vol} and α_2^{vol} provides the foundation for us to devise a small-α approach that is used to avoid the volumetric locking for the overestimation problems by using any $\alpha_1^{\text{vol}} \leq \alpha \leq \alpha_2^{\text{vol}}$. Note that for the underestimation problems, the numerical stability of the solution at $\alpha = 0.0$ is ensured due to excessive displacement constraints. It is therefore both the zero-α approach or the small-α approach can be used to avoid the volumetric locking for underestimation problems.

Note that, for this kind of problems, we have to give up on the "exact" solution, and only focus on solving the volumetric locking.

6 Numerical examples

In this section, four numerical examples will be analyzed using the αFEM. The two first examples are used to illustrate the important properties of the αFEM when the strain energy of the solution at $\alpha = 0.0$ is an overestimation of the exact solution, while two examples are for the case when the strain energy of the solution at $\alpha = 0.0$ is an underestimation of the exact solution.

In order to study the convergence rate of the present method, two norms are used here, i.e., displacement error norm and energy error norm. The displacement error norm is given by Eq. (44) and the energy error norm is defined by

$$e_e(\alpha) = |E(\alpha) - E_{\text{exact}}|^{1/2} \tag{45}$$

Table 10 Eigenvalues of a free solid using one element ($E = 3.0 \times 10^7$, $\nu = 0.499999$)

Eigen values	1	2	3	4	5	6	7	8
$\alpha = 0.0$	0	0	0	0	0	1.99 e+07	2.01 e+07	1.00 e+13
$\alpha = (0.5 - \nu)\, e - 02$ (or $\alpha = 1e$-08)	0	0	0	0	0	1.99 e+07	2.01 e+07	1.00 e+13
$\alpha = (0.5 - \nu)\, e - 01$ (or $\alpha = 1e$-07)	0	0	0	0	0	1.99 e+07	2.01 e+07	1.00 e+13
$\alpha = (0.5 - \nu)$ (or $\alpha = 1e - 06$)	0	0	0	1.50	2.00	1.99 e+07	2.01 e+07	1.00 e+13
$\alpha = (0.5 - \nu)\, e + 01$ (or $\alpha = 1e - 05$)	0	0	0	1.54 e+02	1.96 e+02	1.99 e+07	2.01 e+07	1.00 e+13
$\alpha = (0.5 - \nu)\, e + 02$ (or $\alpha = 1e - 04$)	0	0	0	1.54 e+04	1.96 e+04	1.99 e+07	2.01 e+07	1.00 e+13
$\alpha = 1.0$	0	0	0	1.84 e+07	1.87 e+07	1.83 e+12	2.11 e+12	1.02 e+13

Table 11 Eigenvalues of a free solid using one element ($E = 3.0 \times 10^7$, $\nu = 0.49999$)

Eigen values	1	2	3	4	5	6	7	8
$\alpha = 0.0$	0	0	0	0	0	1.99 e+07	2.01 e+07	1.00 e+12
$\alpha = (0.5 - \nu)\, e - 02$ (or $\alpha = 1e - 07$)	0	0	0	0	0	1.99 e+07	2.01 e+07	1.00 e+12
$\alpha = (0.5 - \nu)\, e - 01$ (or $\alpha = 1e - 06$)	0	0	0	0.15	0.20	1.99 e+07	2.01 e+07	1.00 e+12
$\alpha = (0.5 - \nu)$ (or $\alpha = 1e - 05$)	0	0	0	1.54 e+01	1.96 e+01	1.99 e+07	2.01 e+07	1.00 e+12
$\alpha = (0.5 - \nu)\, e + 01$ (or $\alpha = 1e - 04$)	0	0	0	1.54 e+03	1.96 e+03	1.99 e+07	2.01 e+07	1.00 e+12
$\alpha = (0.5 - \nu)\, e + 02$ (or $\alpha = 1e - 03$)	0	0	0	1.54 e+05	1.95 e+05	1.99 e+07	2.01 e+07	1.00 e+12
$\alpha = 1.0$	0	0	0	1.84 e+07	1.87 e+07	1.83 e+11	2.11 e+11	1.02 e+12

Table 12 Eigenvalues of a free solid using one element ($E = 3.0 \times 10^7$, $\nu = 0.4999$)

Eigen values	1	2	3	4	5	6	7	8
$\alpha = 0.0$	0	0	0	0	0	1.99 e+07	2.01 e+07	1.00 e+11
$\alpha = (0.5 - \nu)\, e - 02$ (or $\alpha = 1e - 06$)	0	0	0	0.015	0.020	1.99 e+07	2.01 e+07	1.00 e+11
$\alpha = (0.5 - \nu)\, e - 01$ (or $\alpha = 1e - 05$)	0	0	0	1.54	1.96	1.99 e+07	2.01 e+07	1.00 e+11
$\alpha = (0.5 - \nu)$ (or $\alpha = 1e - 04$)	0	0	0	1.54 e+02	1.96 e+02	1.99 e+07	2.01 e+07	1.00 e+11
$\alpha = (0.5 - \nu)\, e + 01$ (or $\alpha = 1e - 03$)	0	0	0	1.54 e+04	1.96 e+04	1.99 e+07	2.01 e+07	1.00 e+11
$\alpha = (0.5 - \nu)\, e + 02$ (or $\alpha = 1e - 02$)	0	0	0	1.53 e+06	1.94 e+06	2.01 e+07	2.02 e+07	1.00 e+11
$\alpha = 1.0$	0	0	0	1.84 e+07	1.87 e+07	1.83 e+10	2.11 e+10	1.02 e+11

Table 13 Eigenvalues of a free solid using one element ($E = 3.0 \times 10^7$, $\nu = 0.499$)

Eigen values	1	2	3	4	5	6	7	8
$\alpha = 0.0$	0	0	0	0	0	1.99 e+07	2.01 e+07	1.00 e+10
$\alpha = (0.5 - \nu)\, e - 02$ (or $\alpha = 1e - 05$)	0	0	0	0.155	0.196	1.99 e+07	2.01 e+07	1.00 e+10
$\alpha = (0.5 - \nu)\, e - 01$ (or $\alpha = 1e - 04$)	0	0	0	1.55 e+01	1.96 e+01	1.99 e+07	2.01 e+07	1.00 e+10
$\alpha = (0.5 - \nu)$ (or $\alpha = 1e - 03$)	0	0	0	1.55 e+03	1.96 e+03	1.99 e+07	2.01 e+07	1.00 e+10
$\alpha = (0.5 - \nu)\, e + 01$ (or $\alpha = 1e - 02$)	0	0	0	1.55 e+05	1.96 e+05	1.99 e+07	2.01 e+07	1.00 e+10
$\alpha = (0.5 - \nu)\, e + 02$ (or $\alpha = 1e - 01$)	0	0	0	1.30 e+07	1.53 e+07	2.39 e+07	2.58 e+07	1.01 e+10
$\alpha = 1.0$	0	0	0	1.84 e+07	1.87 e+07	1.84 e+09	2.12 e+09	1.02 e+10

Table 14 Condition number of stiffness matrix **K** of a free solid using one element ($E = 3.0 \times 10^7$)

	$\nu = 0.499$	$\nu = 0.4999$	$\nu = 0.49999$	$\nu = 0.499999$
$\alpha = 0.0$	2.805 e+33	3.775 e+33	1.145 e+33	8.839 e+32
$\alpha = (0.5 - \nu)\, e - 02$	1.210 e+17	5.711 e+16	7.827 e+16	9.954 e+22
$\alpha = (0.5 - \nu)\, e - 01$	9.364 e+16	6.429 e+17	2.205 e+17	5.701 e+17
$\alpha = (0.5 - \nu)$	2.411 e+17	5.363 e+16	1.739 e+17	1.887 e+17
$\alpha = (0.5 - \nu)\, e + 01$	3.297 e+17	2.246 e+17	2.338 e+17	1.261 e+17
$\alpha = (0.5 - \nu)\, e + 02$	1.565 e+17	5.081 e+16	1.521 e+17	2.600 e+17
$\alpha = 1.0$	2.400 e+17	1.994 e+17	3.875 e+17	2.226 e+17

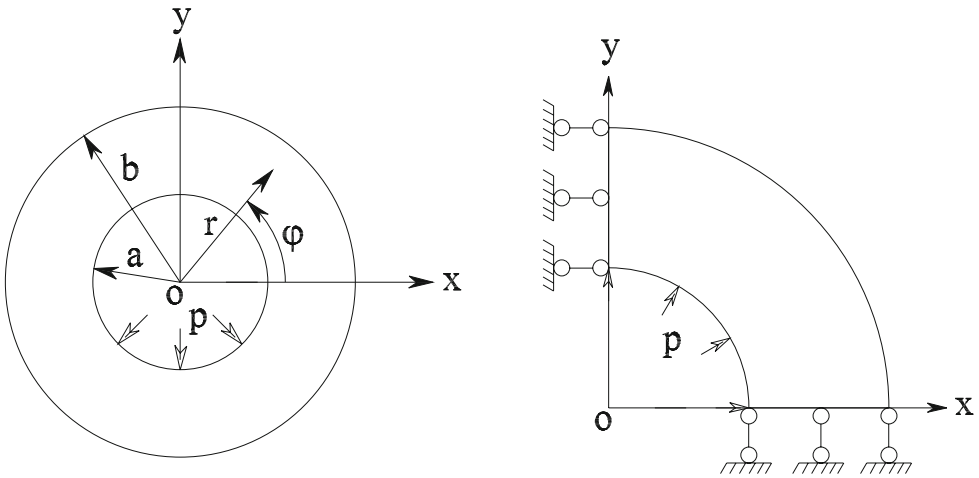

Fig. 4 A thick cylindrical pipe subjected to an inner pressure and its quarter model

where the total strain energy of numerical solution $E(\alpha)$ and the total strain energy of exact solution E_{exact} is calculated by

$$E(\alpha) = \frac{1}{2}\sum_{i=1}^{\text{nel}} \int_{-1}^{1}\int_{-1}^{1} \left(\tilde{\boldsymbol{\varepsilon}}_i^h(\alpha,\xi,\eta)\right)^T \mathbf{D}\,\tilde{\boldsymbol{\varepsilon}}_i^h \times (\alpha,\xi,\eta)\left|\tilde{\mathbf{J}}(\alpha,\xi,\eta)\right| d\xi d\eta \tag{46}$$

$$E_{\text{exact}} = \frac{1}{2}\lim_{\text{nel}\to\infty}\sum_{i=1}^{\text{nel}}\int_{\Omega_i} \boldsymbol{\varepsilon}_i^T \mathbf{D}\,\boldsymbol{\varepsilon}_i d\Omega = \frac{1}{2}\lim_{\text{nel}\to\infty}\sum_{i=1}^{\text{nel}}\int_{-1}^{1}\int_{-1}^{1} \boldsymbol{\varepsilon}_i^T \mathbf{D}\,\boldsymbol{\varepsilon}_i \left|\mathbf{J}(\xi,\eta)\right| d\Omega \tag{47}$$

where nel is the total number of element of the problem, $\boldsymbol{\varepsilon}_i$ and $\tilde{\boldsymbol{\varepsilon}}_i^h$ are the strain of exact solution and the strain of numerical solution of the ith element, respectively. In actual computation using Eq. (47), we will use a very fine mesh (nel $\to \infty$) to calculate the exact strain energy E_{exact}.

6.1 A cylindrical pipe subjected to an inner pressure: exact-α approach

Figure 4 shows a thick cylindrical pipe, with internal radius $a = 0.1$ m, external radius $b = 0.2$ m, subjected to an internal pressure $p = 6\,\text{kN/m}^2$. Because of the axi-symmetric characteristic of the problem, we only calculate for one quarter of cylinder as shown in Fig. 4. Figure 5 gives the discretization of the domain using 4-node quadrilateral elements. Plane strain condition is considered and Young's modulus $E = 21000\,\text{kN/m}^2$, Poisson's ratio $\nu = 0.3$. Symmetric conditions are imposed on the left and bottom edges, and outer boundary is traction free. The exact solution for the stress components is [39]

$$\sigma_r(r) = \frac{a^2 p}{b^2 - a^2}\left(1 - \frac{b^2}{r^2}\right);$$
$$\sigma_\varphi(r) = \frac{a^2 p}{b^2 - a^2}\left(1 + \frac{b^2}{r^2}\right); \tag{48}$$
$$\sigma_{r\varphi} = 0$$

while the radial and tangential exact displacements are given by

$$u_r(r) = \frac{(1+\nu)\,a^2 p}{E\left(b^2 - a^2\right)}\left\{(1-2\nu)\,r + \frac{b^2}{r}\right\}; \quad u_\varphi = 0 \tag{49}$$

where (r, φ) are the polar coordinates and α is measured counter-clockwise from the positive x-axis.

Table 15 shows, respectively, the results of condition number, strain energy, error norms of displacement and energy using the mesh (4×8) for $\alpha \in [0, 1]$. The results show that at $\alpha = 0.0$ the hour-glass phenomenon or zero-energy

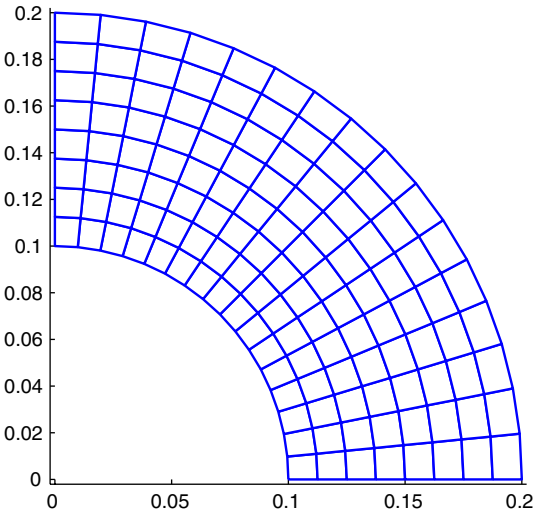

Fig. 5 Discretization of the domain using 4-node quadrilateral elements

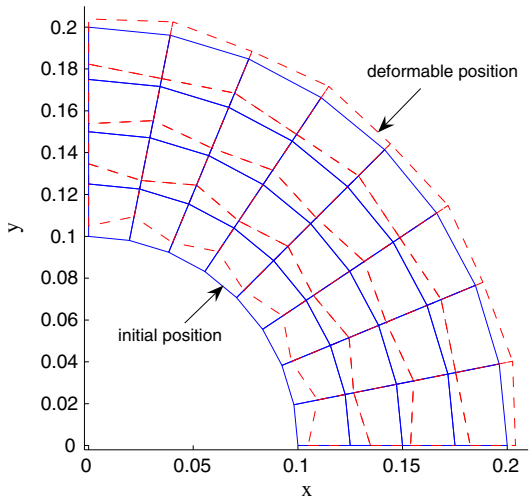

Fig. 6 Hour-glass phenomenon or zero-energy modes appear at $\alpha = 0.0$ (mesh 4×8)

modes appear as shown in Fig. 6. The stiffness matrix with the boundary conditions imposed is nearly singular. As a result, the condition number and displacement error norm are very big compared to those of other values of α. This problem can be easily overcome by using $\alpha \geq \alpha_1^{\text{sta}} = 1e-03$ which show that the condition number decreases sharply to the value which is comparable to $\alpha = 1.0$ (standard FEM with full integration). As a result, the hour-glass phenomenon and zero-energy modes disappear as shown in Fig. 7 at $\alpha = \alpha_1^{\text{sta}}$ and displacement error norm also decreases sharply to the value which is comparable to $\alpha = 1.0$. These properties are also similar for meshes (6×12) and (8×16).

We now use the exact-α approach to find the exact solution. Figs. 8, 9 and 10 show, respectively, the strain energy, the error norms of energy and displacement of the cylindrical pipe using three meshes (4×8), (6×12) and (8×16) for $\alpha \in [0, 1]$. Figure 8 shows that the αFEM solution (in strain energy) at $\alpha = 0.0$ is an overestimation of the exact solution, because the strain energy $E(\alpha = 0.0)$ of a fine mesh is smaller than that of a coarse mesh. As an expected result from Theorem 2, there exists a value of α_{exact} such that $E(\alpha_{\text{exact}}) = E_{\text{exact}}$ for each mesh used. The results in Fig. 8 show that the values of $\alpha_{\text{exact}} \approx 0.7065$ of three meshes used are almost coincided at the exact energy E_{exact} (obtained using a fine mesh of 50×100), and in Figs. 9 and 10, both

Table 15 Condition number, strain energy, error norms of displacement and energy (mesh 4×8 - Exact strain energy = 0.2567e−04)

α	Condition number of **K**	Strain energy* 1.0e−04	Displacement error norm (%)	Energy error norm* 1.0e−03	Remarks
0.0 (FEM(G = 1))	1.111 e+18	0.258369965	35.708734	0.4084384	Hour-glass locking
1e−04	0. 874 e+09	0.258369965	0.645454	0.4084384	Less well conditioned
1e−03	0.874 e+07	0.258369961	0.645453	0.4084379	Locking free (well-conditioned)
1e−02	0.601 e+07	0.258369629	0.6453	0.4083973	//
0.1	0.594 e+07	0.25833	0.6338	0.4043	//
0.2	0.589 e+07	0.25823	0.5990	0.3917	//
0.3	0.584 e+07	0.2581	0.5411	0.3697	//
0.4	0.578 e+07	0.2578	0.4601	0.3366	//
0.5	0.570 e+07	0.2575	0.3561	0.2885	//
0.6	0.561 e+07	0.2572	0.2293	0.2159	//
0.7	0.550 e+07	0.2567	0.0798	0.0584	//
0.8	0.538 e+07	0.2562	0.0921	0.2151	//
0.9	0.526 e+07	0.2557	0.2863	0.3199	//
1.0 (FEM(G = 4))	0.514 e+07	0.2551	0.5024	0.4060	//

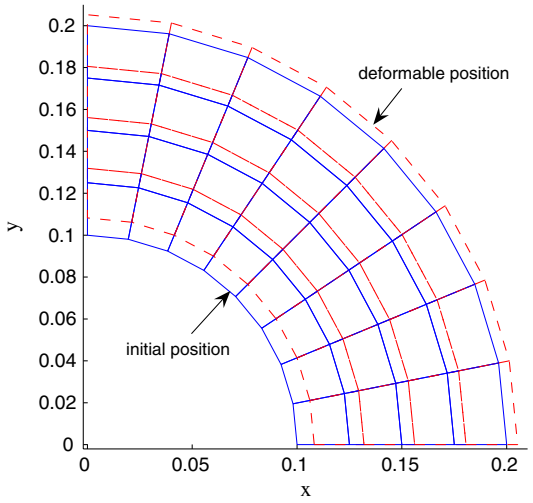

Fig. 7 Hour-glass phenomenon or zero-energy modes disappear at $\alpha = 0.001$(mesh 4×8)

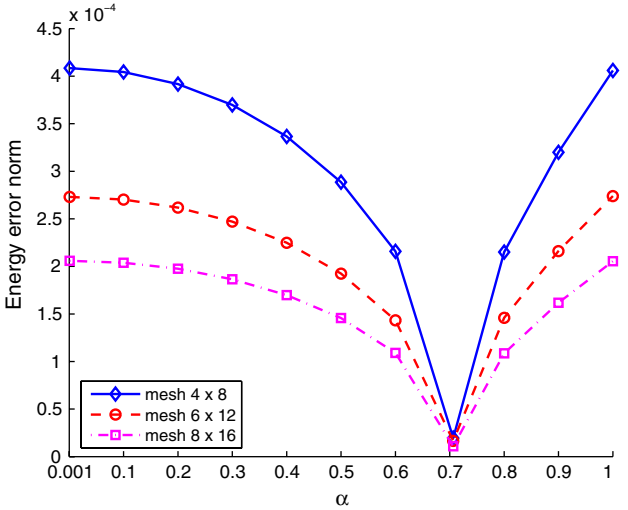

Fig. 9 Energy error norm of the cylindrical pipe subjected to an inner pressure

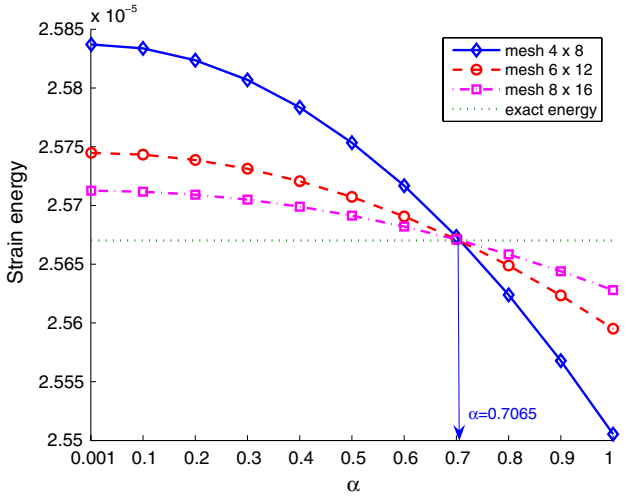

Fig. 8 Strain energy of the cylindrical pipe subjected to an inner pressure

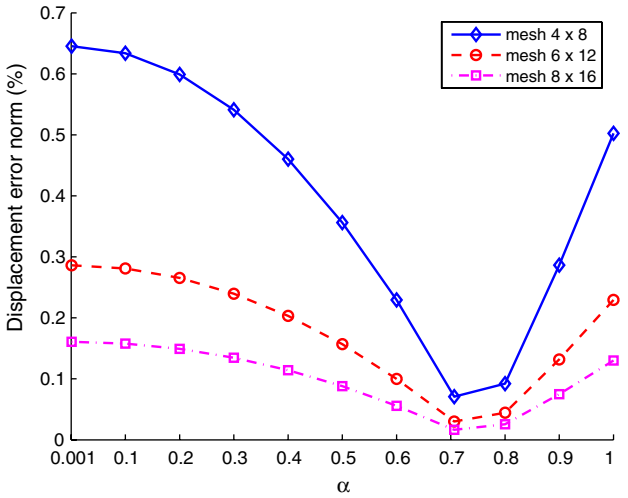

Fig. 10 Displacement error norm (%) of the cylindrical pipe subjected to an inner pressure

error norms of displacement and energy gain the minimum values at $\alpha_{\text{exact}} \approx 0.7065$.

Note that the meshes (4×8), (6×12) and (8×16) used in the computation have the same aspect ratio, which is $1/2$, between the number of elements along the radius-direction and those along the tangent-direction. This ensures the set of three strain energy curves to intersect each other at a common point α_{exact}. If we use another set of three other meshes of a different aspect ratio, for example (4×6), (6×9) and (8×12) which have the same aspect ratio of 2/3, the set of strain energy curves of these three meshes will intersect each other at another intersection, and α_{exact} will have different value as shown in Fig. 11.

Figures 12 and 13 show the convergence rates of error norms of energy and displacement at values of $\alpha \in \{1e-03, \alpha_{\text{exact}}, 1.0\}$. The results show that the error norms of energy and displacement at $\alpha_{\text{exact}} \approx 0.7065$ are much more accurate than those at $\alpha_1^{\text{sta}} = 1e-03$ and $\alpha = 1.0$. In particular, the error norms of energy and displacement at $\alpha_{\text{exact}} \approx 0.7065$ using the coarsest mesh are also much more accurate than those at $\alpha_1^{\text{sta}} = 1e-03$ and $\alpha = 1.0$ using the finest mesh. The convergence rate of displacement is always approximated 2.0 for all three values of α as shown in Fig. 13. The convergence rates of the energy error norm are approximated 1.0 at $\alpha_1^{\text{sta}} = 1e-03$ and $\alpha = 1.0$, but it is almost zero at $\alpha_{\text{exact}} \approx 0.7065$ as shown in Fig. 12. This shows that at α_{exact}, the strain energy computed using the αFEM is the nearly exact value that is not mesh dependent and can not be improved further by mesh refinement.

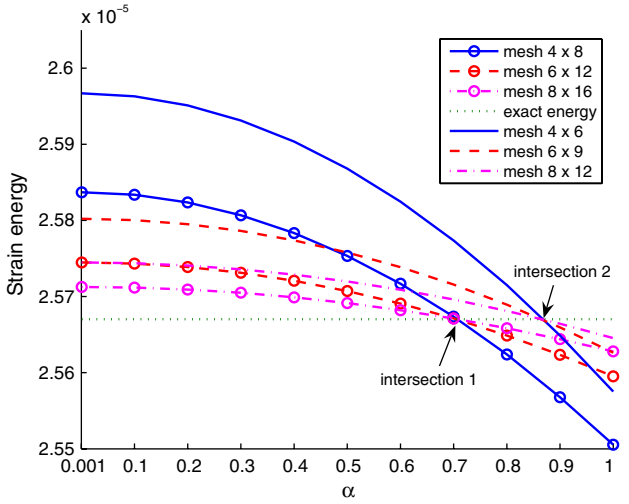

Fig. 11 Strain energy of the cylindrical pipe subjected to an inner pressure

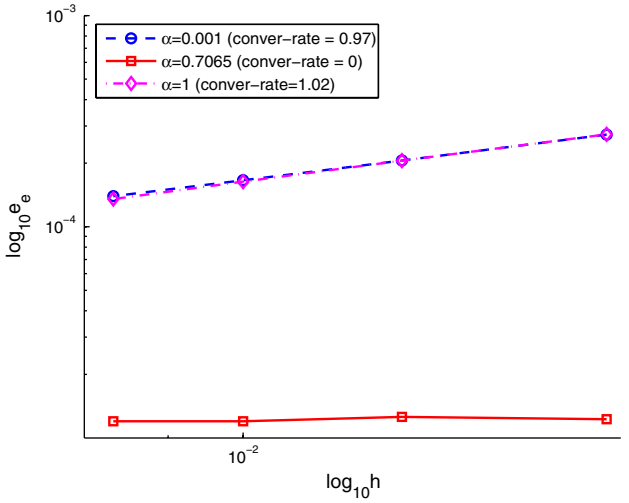

Fig. 12 The convergence rate of energy error norm at the values of $\alpha \in \{0.001,\ \alpha_{\text{exact}},\ 1.0\}$

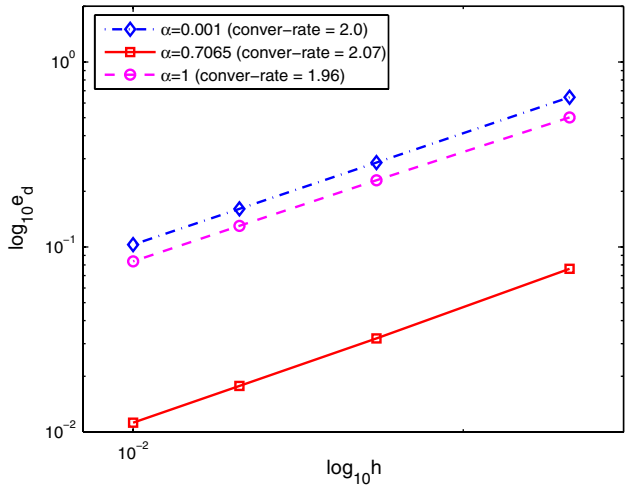

Fig. 13 The convergence rate of displacement error norm at the values of $\alpha \in \{0.001,\ \alpha_{\text{exact}},\ 1\}$

Figure 14 shows the strain energy for $\alpha \in [-70,\ 70]$ and $\alpha \in [-1,\ 1]$ obtained using three meshes 4×8, 6×12 and 8×16. The results verify clearly that the strain energy of the αFEM is a fourth order function of α and there exists a local extreme at $\alpha = 0.0$. Three diagrams intersect each other at two common points inside of $[-1,\ 1]$ where $E = E_{\text{exact}}$. For this problem, the α_{exact} can be also determined using the procedure given in Sect. 4.6.

6.2 αFEM for volumetric locking—problem I (small-α approach)

Next, we will use the αFEM to deal with the problems with nearly incompressible material. The same example problem defined in Sect. 6.1 is used, and all the input data are kept unchanged, except ν is changed from 0.499 to 0.499999. Because this is an overestimation problem, the small-α approach with $\alpha_1^{\text{vol}} = (0.5 - \nu)$ and $\alpha_2^{\text{vol}} = (0.5 - \nu)\, e + 01$ is used to calculate. The results are also compared with those of other values of α.

Tables 16, 17 and 18 show, respectively, the results of displacement error norm, strain energy and condition number $\mathbf{K}$ for the mesh (4×8). The results show that at $\alpha = 0.0$ the hour-glass phenomenon appears, and the condition number and displacement error norm are very big compared to those of other values of α. At $\alpha = 1.0$, the volumetric locking phenomenon appears. Strain energy is much less than the exact strain energy and displacement error norm increase drastically. At $\alpha = (0.5 - \nu)\, e - 02$ and $\alpha = (0.5 - \nu)\, e - 01$, less well conditioned phenomenon appears and increases when ν approaches closer to 0.5. When the small-α approach with $\alpha_1^{\text{vol}} = (0.5 - \nu)$ and $\alpha_2^{\text{vol}} = (0.5 - \nu)\, e + 01$ is used, the results become very good. There are neither ill-conditioning, nor volumetric locking. It therefore verifies that the small-α approach with $\alpha_1^{\text{vol}} \le \alpha \le \alpha_2^{\text{vol}}$ can avoid the volumetric locking and ensure the numerical stability for the overestimation problems.

6.3 Cook's membrane: exact-α approach

This is also a widely used benchmark problem: a clamped tapered panel subjected to an in-plane shearing load resulting in deformation dominated by a bending response, shown in Fig. 15, known Cook's membrane problem [12]. The parameters used are Young's modulus $E = 1$, Poisson's ratio $\upsilon = 1/3$. The exact solution of the problem is unknown. Under plane stress conditions, the reference value of the vertical displacement at center tip section is 23.9642 [14] and the reference value of the strain energy is 12.015 [29]. Use the

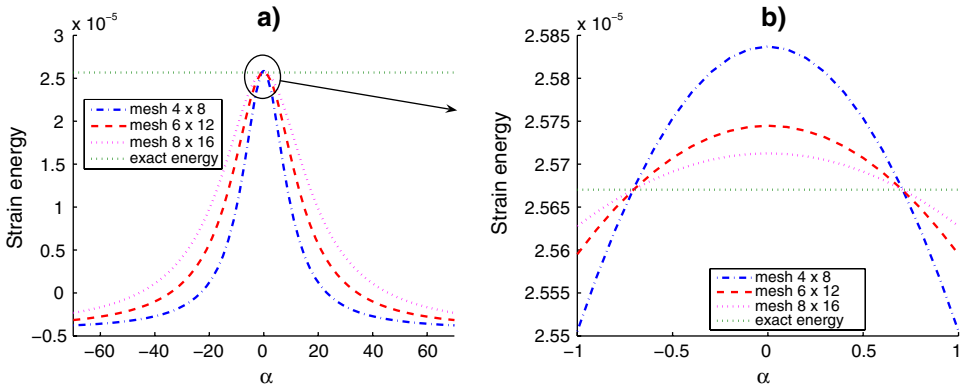

Fig. 14 The strain energy obtained using three meshes 4×8, 6×12 and 8×16 **a** $\alpha \in [-70, 70]$; **b** $\alpha \in [-1, 1]$

Table 16 Displacement error norm (%) (mesh 4×8)

	$\nu = 0.499$	$\nu = 0.4999$	$\nu = 0.49999$	$\nu = 0.499999$	Remarks
$\alpha = 0.0$	185.41	159.84	165.25	187.84	Hour-glass locking
$\alpha = (0.5 - \nu)\, e - 02$	0.645	0.645	0.652	24.182	Less well conditioned
$\alpha = (0.5 - \nu)\, e - 01$	0.645	0.645	0.645	0.642	Locking free
$\alpha = (0.5 - \nu)$	0.645	0.645	0.645	0.645	//
$\alpha = (0.5 - \nu)\, e + 01$	0.630	0.644	0.645	0.645	//
$\alpha = (0.5 - \nu)\, e + 02$	0.922	0.487	0.630	0.644	//
$\alpha = 1.0$	61.05	94.01	99.37	99.94	Volumetric locking

Table 17 Energy strain $(* e - 05)$(mesh 4×8)

	$\nu = 0.499$	$\nu = 0.4999$	$\nu = 0.49999$	$\nu = 0.499999$	Remarks
$\alpha = 0.0$	2.7097	2.7101	2.7102	2.7102	
$\alpha = (0.5 - \nu)\, e - 02$	2.7097	2.7101	2.7102	2.7102	
$\alpha = (0.5 - \nu)\, e - 01$	2.7097	2.7101	2.7102	2.7102	
$\alpha = (0.5 - \nu)$	2.7097	2.7101	2.7102	2.7102	
$\alpha = (0.5 - \nu)\, e + 01$	2.7093	2.7101	2.7102	2.7102	
$\alpha = (0.5 - \nu)\, e + 02$	2.6675	2.7059	2.7097	2.7101	
$\alpha = 1.0$	1.0475	0.1612	0.0170	0.0017	Volumetric locking
Exact energy	2.7093	2.7097	2.7098	2.7098	

Table 18 Condition number **K** (mesh 4×8)

	$\nu = 0.499$	$\nu = 0.4999$	$\nu = 0.49999$	$\nu = 0.499999$	Remarks
$\alpha = 0.0$	4.482 e+17	2.854 e+18	1.348 e+18	5.506 e+17	Hour-glass locking
$\alpha = (0.5 - \nu)\, e - 02$	1.167 e+11	1.169 e+13	1.171 e+15	1.037 e+17	Less well conditioned
$\alpha = (0.5 - \nu)\, e - 01$	1.167 e+09	1.169 e+11	1.169 e+13	1.173 e+15	Less well conditioned
$\alpha = (0.5 - \nu)$	8.009 e+08	7.997 e+09	1.169 e+11	1.169 e+12	Well cconditioned
$\alpha = (0.5 - \nu)\, e + 01$	7.905 e+08	7.961 e+09	7.991 e+10	7.995 e+11	//
$\alpha = (0.5 - \nu)\, e + 02$	6.836 e+08	7.735 e+09	7.889 e+10	7.959 e+11	//
$\alpha = 1.0$	9.853 e+08	1.220 e+10	1.268 e+11	1.273 e+12	//

exact α-approach of the αFEM, we found $\alpha_{\text{exact}} = 0.2547$ at the intersection of two strain energy curves using two meshes with the same aspect ratio (64 and 144 elements), as shown in Fig. 16. The solutions at $\alpha_{\text{exact}} = 0.2547$ are 23.962 for the tip displacement and 12.014 for strain energy, which agree very well with the reference solution.

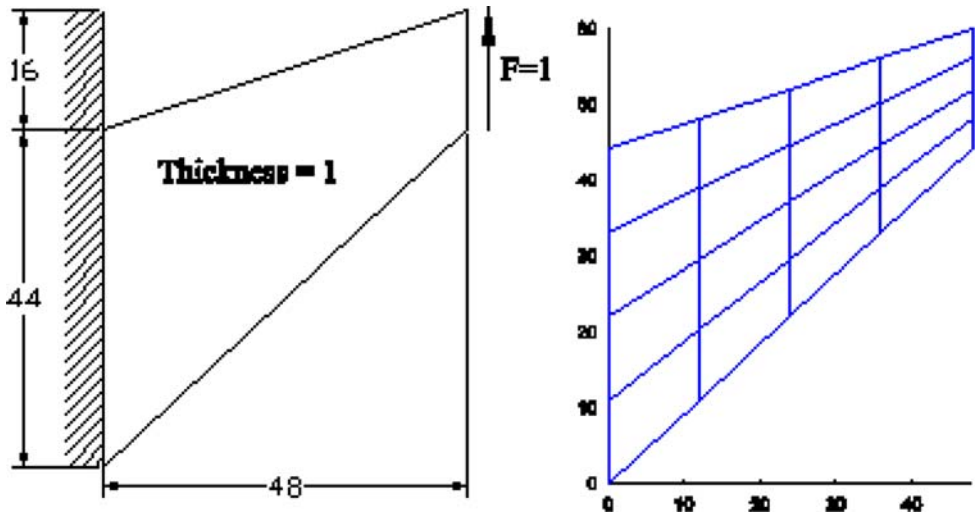

Fig. 15 Cook's membrane problem and its discretization with the coarse mesh

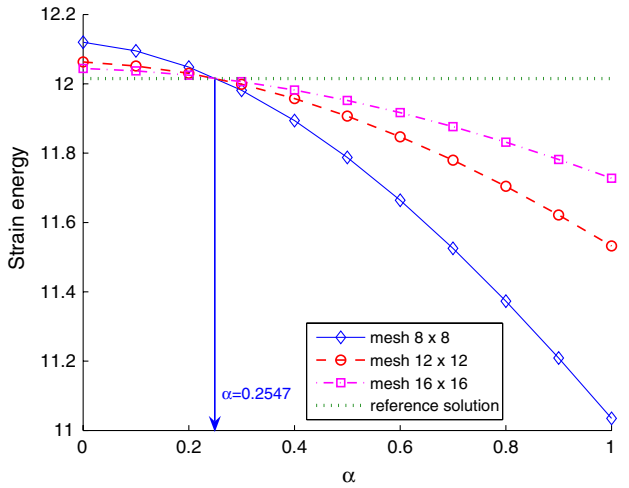

Fig. 16 Strain energy of the Cook's problem ($\nu = 1/3$)

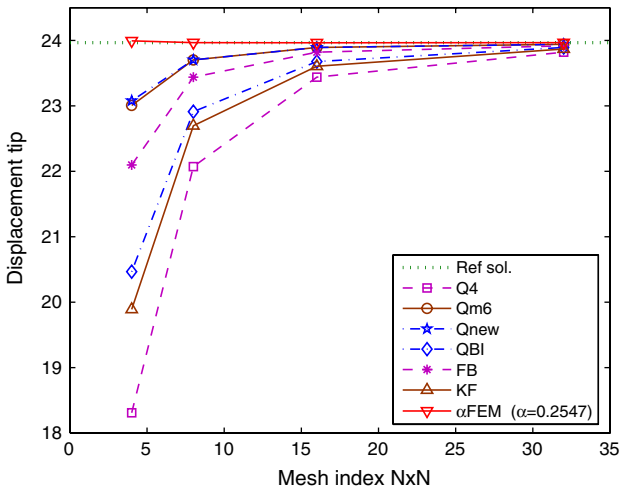

Fig. 17 Convergence of displacement tip for Cook's membrane ($\nu = 1/3$)

Figure 17 compares the result of the tip displacement of the αFEM with six published 4-node quadrilateral elements: Q4-standard isoparametric 2×2 quadrature Gauss points, Qm6-modified Wilson element [38], FB-one Gauss point with hourglass stabilization [13], QBI-Quintessential bending/incompressible element [5], KF-one Gauss point with hour-glass control [20] and Qnew—an improved stabilization technique for one-point quadrature integration method [14]. It can be seen that the result of the αFEM at $\alpha = 0.2547$ is much more accurate than all those of other elements with coarse meshes.

In addition to the results shown in Fig. 17, we also make comparison of the αFEM with other elements for coarse meshes, and the results in numbers are listed in Table 19: Allman's membrane triangle (AT) [1], assumed stress hybrid methods such as Pian–Sumihara's element (P–S) [31], HQM/HQ4 element [40], Zhou–Nie's element (CH(0–1)) [42] and Xie–Zhou's element (ECQ4/LQ6) [41], finite element primal–mixed approach (FEMIXHB) introduced by Mijuca et al. [29], QGA6-I and QGA6-II—the membrane elements using the quadrilateral area coordinate approach by Chen et al. [10], QACM4—the membrane elements using the quadrilateral area coordinate approach by Cen et al. [9] and QACII6—the membrane elements using the new quadrilateral area coordinate method by Chen et al. [11]. It is found that the αFEM gives the best results compared to other elements, especially in term of strain energy.

6.4 Infinite plate with a circular hole (zero-α approach)

Figure 18 represents a plate with a central circular hole of radius $a = 1$ m, subjected to a unidirectional tensile load of $\sigma = 1.0$N/m at infinity in the x-direction. Due to its symmetry, only the upper right quadrant of the plate is modeled. Plane strain condition is considered. Symmetric conditions

Table 19 Results of displacement tip and strain energy for Cook's problem

	Displacement tip			Strain energy		
	2 × 2	4 × 4	8 × 8	2 × 2	4 × 4	8 × 8
AT	19.67 (27)*	22.41 (75)	23.45 (243)	9.84	11.22	11.75
P-S	21.13 (18)	23.02 (50)	23.69 (162)	10.50	11.51	11.85
CH(0 – 1)	23.01 (18)	23.48 (50)	23.81 (162)	11.47	11.75	11.91
ECQ4/LQ6	23.05 (18)	23.48 (50)	23.81 (162)	11.48	11.75	11.91
HMQ/HQ4	21.35 (18)	23.04 (50)	23.69 (162)	10.61	11.52	11.85
FEMIXHB	22.81 (35)	23.52 (135)	23.92 (527)	11.27	11.79	11.97
AGQ6-I	23.07	23.68	23.87	–	–	–
AGQ6-II	25.92	24.37	24.04	–	–	–
QACM4	20.74	22.99	23.69	–	–	–
QACII6	25.92	24.37	24.04	–	–	–
α **FEM**	24.94 (18)	23.99 (50)	23.966 (162)	12.45	12.068	12.014
Reference value	23.9642	23.9642	23.9642	12.015	12.015	12.015

* Number of degrees of freedom denoted in parenthesis

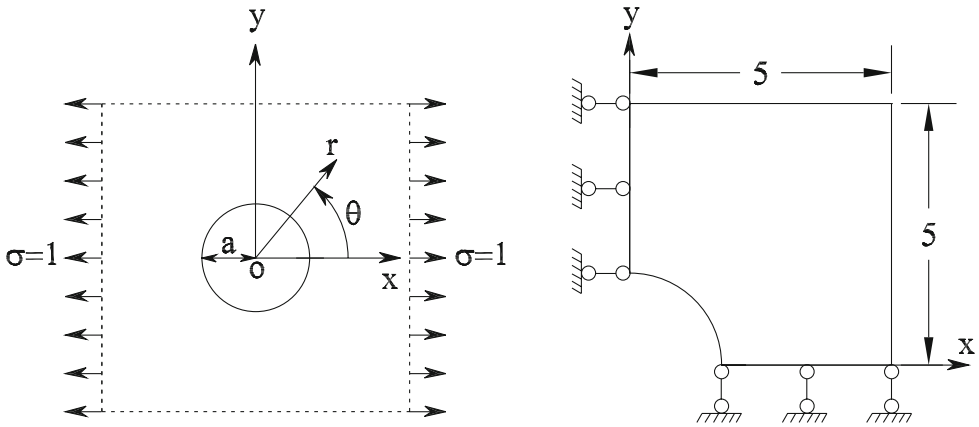

Fig. 18 Infinite plate with a circular hole and its quarter model

are imposed on the left and bottom edges, and the inner boundary of the hole is traction free. The exact solution for the stress is [39]

$$\begin{aligned}
\sigma_{11} &= 1 - \frac{a^2}{r^2}\left[\frac{3}{2}\cos 2\theta + \cos 4\theta\right] + \frac{3a^4}{2r^4}\cos 4\theta \\
\sigma_{22} &= -\frac{a^2}{r^2}\left[\frac{1}{2}\cos 2\theta - \cos 4\theta\right] - \frac{3a^4}{2r^4}\cos 4\theta \\
\tau_{12} &= -\frac{a^2}{r^2}\left[\frac{1}{2}\sin 2\theta + \sin 4\theta\right] + \frac{3a^4}{2r^4}\sin 4\theta
\end{aligned} \tag{50}$$

where (r, θ) are the polar coordinates and θ is measured counterclockwise from the positive x-axis. Traction boundary conditions are imposed on the right ($x = 5.0$) and top ($y = 5.0$) edges based on the exact solution Eq. (50). The displacement components corresponding to the stresses are

$$\begin{aligned}
u_1 &= \frac{a}{8\mu}\left[\frac{r}{a}(\kappa+1)\cos\theta + 2\frac{a}{r}((1+\kappa)\cos\theta + \cos 3\theta)\right. \\
&\quad \left. -2\frac{a^3}{r^3}\cos 3\theta\right] \\
u_2 &= \frac{a}{8\mu}\left[\frac{r}{a}(\kappa-1)\sin\theta + 2\frac{a}{r}((1-\kappa)\sin\theta + \sin 3\theta)\right. \\
&\quad \left. -2\frac{a^3}{r^3}\sin 3\theta\right]
\end{aligned} \tag{51}$$

where $\mu = E/(2(1+\nu))$, κ is defined in terms of Poisson's ratio by $\kappa = 3 - 4\nu$ for plane strain cases.

Figure 19 gives the discretization of the domain using 4-node quadrilateral elements. Figures 20, 21 and 22 show, respectively, the strain energy, the error norms of energy and displacement of the infinite plate with a circular hole using three meshes (12 × 12), (16 × 16) and (20 × 20) for $\alpha \in [0, 1]$. It is clear from Fig. 20 that the αFEM solution (in strain energy) at $\alpha = 0.0$ is an underestimation of the exact

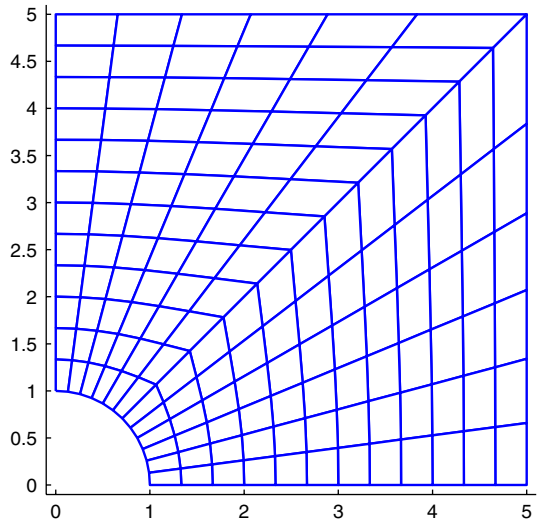

Fig. 19 Domain discretization of the infinite plate with a circular hole using 4-node quadrilateral elements

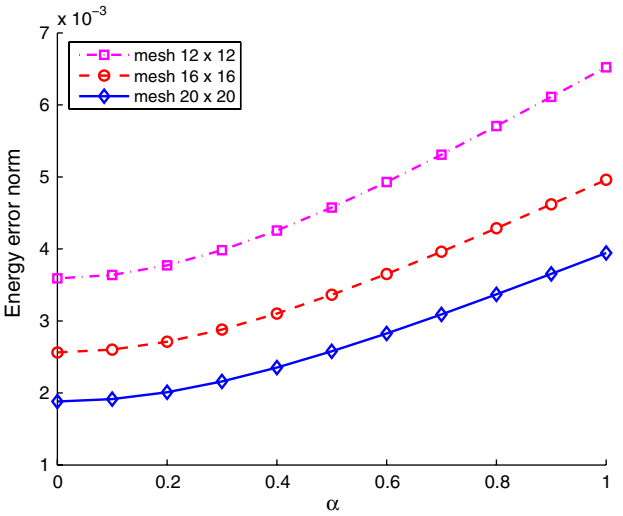

Fig. 21 Energy error norm of the infinite plate with a circular hole

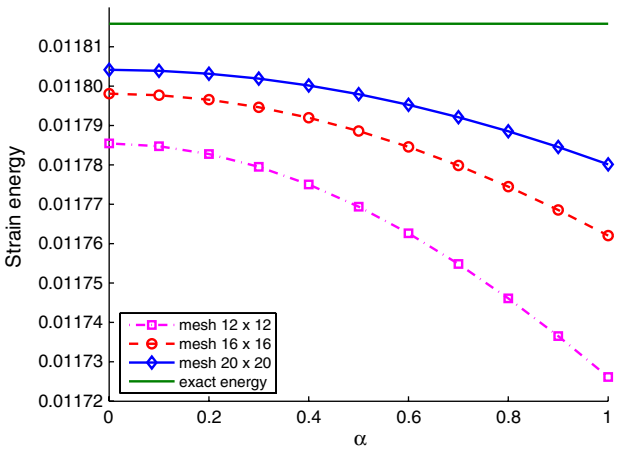

Fig. 20 Strain energy of the infinite plate with a circular hole

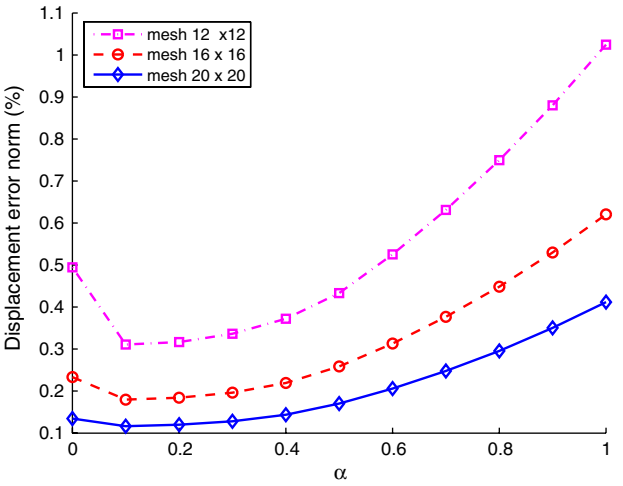

Fig. 22 Displacement error norm (%) of the infinite plate with a circular hole

solution, because the strain energy E ($\alpha = 0.0$) of a fine mesh is larger than that of a coarse mesh. As an expected result from Theorem 3, the strain energy at $\alpha = 0.0$ is closest to the exact energy for each mesh used. The standard FEM is impossible to predict this. The results in Fig. 20 also show that the computed strain energy is always an underestimation of the exact energy (obtained using a fine mesh of 80×80) for any $\alpha \in [0,\ 1]$, and the strain energy approaches to the exact strain energy from below when the mesh becomes finer. In this case, the energy-α curves do not intersect each other and the energy error norm obtains the minimum value at $\alpha = 0.0$ as shown in Fig. 21. The displacement norm obtains the minimum value at a little different value of α (here at $\alpha \approx 0.1$ as shown in Fig. 22). Note that there is no hour-glass mode at $\alpha = 0.0$ in this case as this is an underestimation problem.

The above results show that if the energy at $\alpha = 0.0$ is an underestimation of the exact energy, we only have the basis to choose the solution with the best energy error norm (at $\alpha = 0.0$). The choice of α for the best displacement solution is not obvious.

6.5 Connecting bar: a practical application: (zero-α approach)

This example performs a static analysis of an automobile part, a connecting bar with a relatively complex configuration, as shown in Fig. 23. The boundary conditions as well as the applied load are demonstrated in this figure with $p = 1\,\text{MPa}$. Plane stress problem is considered with elastic modulus $E = 10\,\text{GPa}$ and Poisson's ratio $\nu = 0.3$.

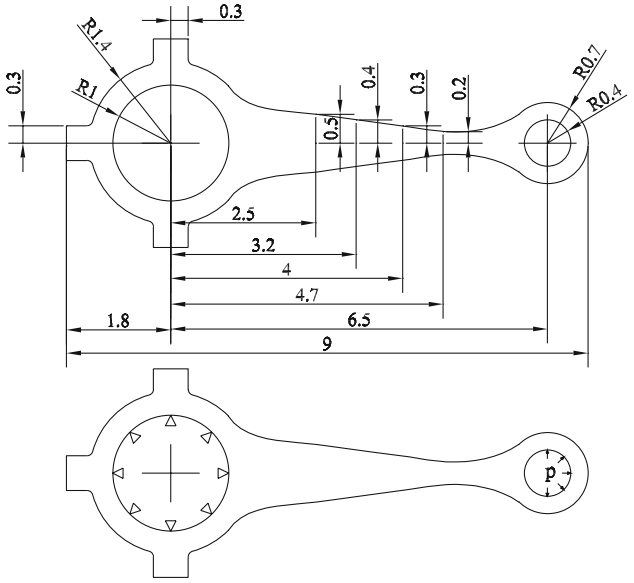

Fig. 23 Geometric model and boundary conditions of an automobile connecting bar

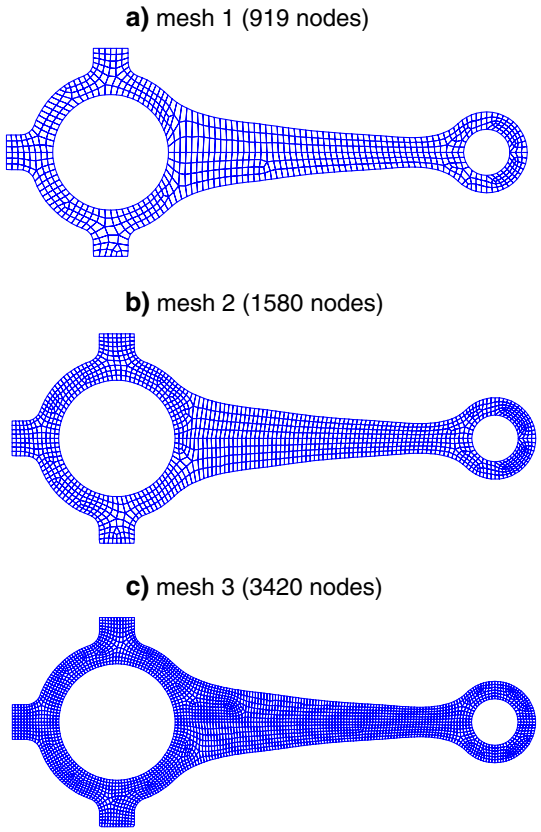

Fig. 24 Domain discretization of the connecting bar using three meshes **a** Mesh 1 (919 nodes); **b** Mesh 2 (1580 nodes); **c** Mesh 3 (3420 nodes)

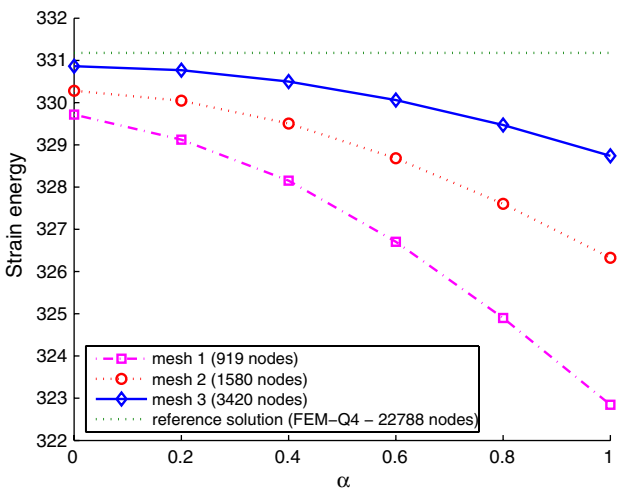

Fig. 25 Strain energy of the connecting bar

Figure 24 gives the discretization of the domain using 3 meshes (919, 1580 and 3420 nodes) with 4-node quadrilateral elements. As no closed form solutions are available, a reference solution is obtained using the standard FEM with 22788 nodes.

Figure 25 shows the strain energy of the connecting bar using three meshes (919, 1580 and 3420 nodes) for $\alpha \in [0,\ 1]$, respectively. The results also show the same properties as those of the infinite plate with a circular hole. The αFEM solution (in strain energy) at $\alpha = 0.0$ is an underestimation of the exact solution, because the strain energy E ($\alpha = 0.0$) of a finer mesh is larger than that of a coarser mesh. As an expected result from Theorem 3, the strain energy at $\alpha = 0.0$ is closest to the exact energy for each mesh used. The computed strain energies are always an underestimation of the reference strain energy obtained using the standard FEM with 22788 nodes for any $\alpha \in [0,\ 1]$, and these strain energies approaches to the reference strain energy when the meshes become finer.

7 Conclusion

In this work, we propose the αFEM based on the framework of FEM but incorporating the strain and Jacobian matrix with a scaling factor α. Through the theoretical analyses, formulations and numerical examples, some conclusions can be drawn as follows:

1. The αFEM gives a continuous form of the solutions ranging from the standard FEM using the reduced integration to the standard FEM using the full Gauss integration by changing the parameter α from 0.0 to 1.0. By using $0.0 \leq \alpha < 1.0$, the αFEM can reduce the overestimation of the stiffness matrix of standard FEM model and produce much more stable and accurate solution without increasing computational cost.

2. The strain energy of the solutions in the αFEM is a fourth order function of the scaling factor α. This strain energy function with $\alpha \in [0, 1]$ is finite and bounded from above and below by the strain energies E ($\alpha = 0.0$) and E ($\alpha = 1.0$), respectively. This implies that the αFEM with $\alpha \in [0, 1]$ is energy consistent and capable of reproduce exactly all linear fields, and hence converges to any continuous fields.
3. A simple approach has been proposed to determine where the problem is: overestimation or underestimation problems. For overestimation problems, the exact-α approach is proposed to determine an α_{exact} at which the solution of the strain energy is exact and the error norm of displacement of the solution obtains its minimum. The error norms of energy and displacement at α_{exact} using a very coarse mesh are significantly more accurate than those at $\alpha = 0.0$ and $\alpha = 1.0$ using very fine meshes. For underestimation problems, the zero-α approach is proposed to provide the solution in the strain energy that is closest to the exact solution.
4. For the overestimation problems, the αFEM using $\alpha \in [\alpha_1^{\text{sta}}, \alpha_2^{\text{sta}}]$ for the compressible materials will ensure the numerical stability and the solution in the strain energy is almost the same with that of the FEM using the reduced integration. In addition, using the αFEM with small-α approach ($\alpha \in [\alpha_1^{\text{vol}}, \alpha_2^{\text{vol}}]$) is an effective way to avoid the volumetric locking.
5. Coding of the αFEM is very simple. It is nearly the same as the standard displacement compatible FEM. The changes are only to the strain and Jacobian matrices, and hence can be very easily implemented. The computation cost of the αFEM is the same as the standard FEM with full integration.
6. Comparing to other finite element formulations, like mixed finite elements or under integrated and stabilized elements, the first benefit of the αFEM is that it has general schemes to find the solution with the exact strain energy for the overestimation problems and to find the best possible solution for the underestimation problems. The second benefit of the αFEM is the ease of implementation without much modification to the existing FEM codes. In the αFEM, we only need to determine suitable value α and the numerical procedure is almost similar to that for the standard FEM, while others finite element formulations need special techniques to formulate the stabilization matrix or calculate mixed stiffness matrix.

The ideal of αFEM can be extended to other types of problems, such as 3D problems, geometric and elasto-plastic nonlinear problems, because the implementation procedure in αFEM is quite similar as the FEM. Other types of locking problems can also be delt with properily manipulating the gradient of the field gradient. More works need to be done along this direction.

References

1. Allman DJ (1984) A compatible triangular element including vertex rotations for plane elasticity analysis. Comput Struct 19:1–8
2. Arnold DN (1990) Mixed finite element methods for elliptic problems. Comput Methods Appl Mech Eng 82:281–300
3. Bathe KJ (1996) Finite element procedures. Prentice Hall, Masetchuset
4. Belytschko T, Tsay CS, Liu WK (1981) A stabilization matrix for the bilinear Mindlin plate element. Comput Methods Appl Mech Eng 29:313–327
5. Belytschko T, Bachrach W (1986) Efficient implementation of quadrilaterals with high coarse-mesh accuracy. Comput Methods Appl Mech Eng 54:279–301
6. Belytschko T, Ong JSJ (1984) Hourglass control in linear and nonlinear problems. Comput Methods Appl Mech Eng 43:251–276
7. Belytschko T, Tsay CS (1983) A stabilization procedure for the quadrilateral plate element with one-point quadrature. Int J Numer Methods Eng 19:405–419
8. Brezzi F, Fortin M (1991) Mixed and Hybrid finite element methods. Springer, New York
9. Cen S, Chen XM, Fu XR (2007) Quadrilateral membrane element family formulated by the quadrilateral area coordinate method. Comput Methods Appl Mech Eng 196:4337–4353
10. Chen XM, Cen S, Long YQ, Yao ZH (2004) Membrane elements insensitive to distortion using the quadrilateral area coordinate method. Comput Struct 82(1):35–54
11. Chen XM, Cen S, Fu XR, Long YQ (2007) A new quadrilateral area coordinate method (QACM-II) for developing quadrilateral finite element models. Int J Numer Methods Eng 73:1911–1941
12. Cook R (1974) Improved two–dimensional finite element. J Struct Div ASCE 100(ST6):1851–1863
13. Flanagan DP, Belytschko T (1981) A uniform strain hexahedron and quadrilateral with orthogonal hourglass control. Int J Numer Methods Eng 17:679–706
14. Fredriksson M, Ottosen NS (2004) Fast and accurate 4-node quadrilateral. Int J Numer Methods Eng 61:1809–1834
15. Gruttmann F, Wagner W (2004) A stabilized one-point integrated quadrilateral Reissner–Mindlin plate element. Int J Numer Methods Eng 61:2273–2295
16. Hughes TJR (1980) Generalization of selective integration procedures to anisotropic and nonlinear media. Int J Numer Methods Eng 15:1413–1418
17. Hughes TJR (1987) The finite element method: linear static and dynamic finite element analysis. Prentice-Hall, Englewood Cliffs
18. Johnson C (1987) Numerical solution of partial differential equations by the finite element method. Cambridge University Press, New York
19. Kelly DW (1980) Bounds on discretization error by special reduced integration of the Lagrange family of finite elements. Int J Numer Methods Eng 15:1489–1506
20. Kosloff D, Frazier GA (1978) Treatment of hourglass patterns in low order finite element codes. Int J Numer Anal Methods Geomech 2:57–72
21. Korelc J, Wriggers P (1997) Improved enhanced strain four-node element with Taylor expansion of the shape functions. Int J Numer Methods Eng 40:407–421
22. Liu GR, Dai KY, Nguyen TT (2007) A smoothed finite element method for mechanics problems. Comput Mech 39:859–877

23. Liu GR, Quek SS (2003) The finite element method: a practical course. Butterworth Heinemann, Oxford
24. Liu GR, Nguyen TT, Dai KY, Lam KY (2007) Theoretical aspects of the smoothed finite element method (SFEM). Int J Numer Methods Eng 71:902–930
25. Liu WK, Belytschko T (1984) Efficient linear and nonlinear heat conduction with a quadrilateral element. Int J Numer Methods Eng 20:931–948
26. Liu WK, Hu YK, Belytschko T (1994) Multiple quadrature underintegrated finite elements. Int J Numer Methods Eng 37:3263–3289
27. Liu WK, Ong JSJ, Uras RA (1985) Finite element stabilization matrices—a unification approach. Comp Meths Appl Mech Eng 53:13–46
28. Malkus DS, Hughes TJR (1978) Mixed finite element methods—reduced and selective integration techniques: a unification of concepts. Comp Meth Appl Mech Eng 15:63–81
29. Mijuca D, Berković M (1998) On the efficiency of the primal-mixed finite element scheme. In: Advances in computational structured mechanics. Civil-Comp Press, UK, pp 61–69
30. Nguyen TT, Liu GR, Dai KY, Lam KY (2007) Selective smoothed finite element method. Tsinghua Sci Technol 12(5):497–508
31. Pian THH, Sumihara K (1984) Rational approach for assumed stress finite elements. Int J Numer Methods Eng 20:1685–1695
32. Pian THH, Wu CC (2006) Hybrid and incompatible finite element methods. CRC Press, Boca Raton
33. Reese S, Wriggers P (2000) A stabilization technique to avoid hourglassing in finite elasticity. Int J Numer Methods Eng 48:79–109
34. Rong TY, Lu AQ (2001) Generalized mixed variational principles and solutions for ill-conditioned problems in computational mechanics: Part I. Volumetric locking. Comput Methods Appl Mech Eng 191:407–422
35. Rong TY, Lu AQ (2003) Generalized mixed variational principles and solutions for ill-conditioned problems in computational mechanics: Part II. Shear locking. Comput Methods Appl Mech Eng 192:4981–5000
36. Sandhu RS, Singh KJ (1978) Reduced integration for improved accuracy of finite element approximations. Comp Meths Appl Mech Eng 14:23–37
37. Simo JC, Hughes TJR (1986) On the variational foundations of assumed strain methods. J Appl Mech 53:51–54
38. Taylor RL, Beresford PJ, Wilson EL (1976) A non-conforming element for stress analysis. Int J Numer Methods Eng 10:1211–1219
39. Timoshenko SP, Goodier JN (1970) Theory of elasticity, 3rd edn. McGraw-Hill, New York
40. Xie X (2005) An accurate hybrid macro-element with linear displacements. Commun Numer Methods Eng 21:1–12
41. Xie X, Zhou T (2004) Optimization of stress modes by energy compatibility for 4-node hybrid quadrilaterals. Int J Numer Methods Eng 59:293–313
42. Zhou T, Nie Y (2001) A combined hybrid approach to finite element schemes of high performance. Int J Numer Methods Eng 51:181–202
43. Zienkiewicz OC, Taylor RL (2000) The finite element method, 5th edn. Butterworth Heinemann, Oxford
44. Zienkiewicz OC, Taylor RL, Too JM (1971) Reduced integration technique in general analysis of plates and shells. Int J Numer Methods Eng 3:275–290